Title: Unlocking the Therapeutic Potential of Repaglinide for the Management of Metabolic Syndrome Linked Alzheimer's Disease

1. Introduction:

Metabolic syndrome (MetS) is a condition which includes clusters of metabolic disorders like glucose intolerance, hypertension, dyslipidemia, obesity, insulin resistance, and that together raise the risk of coronary heart disease, diabetes, and stroke. Among all, Type 2 Diabetes Mellitus (T2DM) is the most common cause of mortality and morbidity caused by MetS [1]. According to the International Diabetes Federation, around 537 million people are living with DM, and this number is expected to rise to 783 million by 2045. T2DM is prominently characterized by hyperglycemia due to insulin resistance (IR). It is also associated with various macro and microvascular complications such as diabetic neuropathy, retinopathy, cardiomyopathy, and nephropathy [2]. IR is mediated by reduced insulin receptor expression and dysregulation of signaling cascades such as phosphoinositide 3-kinase (PI3K)/ Glycogen Synthase Kinase-3β (GSK-3β). In the recent past, MetS abnormalities linked to progressive brain insulin resistance (BIR) with consequent impairment of central insulin signaling processes, accumulation of neurotoxins, neuronal stress, and resulting in a progressive course of neurodegeneration which is also termed Type 3 DM [3]. The dysregulated PI3K/GSK-3β in the brain can increase the production and secretion of amyloid-beta (Aβ) and generates hyperphosphorylated tau which prompts neurodegenerative disorders such as Alzheimer's disease (AD). The pathogenesis of AD is multifactorial, with IR and chronic inflammation being key factors in its development [4]. Neurodegeneration in AD is characterized by the deposition of extracellular Aβ plaques and intracellular neurofibrillary tangles composed of hyperphosphorylated tau protein. Moreover, the insulin-degrading enzyme (IDE) plays a crucial role in the clearance of Aβ in the brain, and its dysfunction also has been implicated in the development of AD [5].

Recently, comorbid conditions including DM linked with AD are mounting at an alarming rate and have become a major health issue in developing and developed countries. Although, several treatment options are available for T2DM management which can temporarily delay or reduce the symptoms of the disease including the classes of drugs- Dipeptidyl Peptidase-4 (DPP-4) inhibitors, Sodium-glucose Cotransporter-2 (SGLT2) inhibitors, etc but they are effectively unable to control the diabetic complications and co-morbidities [6]. However, recent pre-clinical and clinical studies have indicated the benefits of the meglitinides class of drugs not only in DM but also in comorbid conditions like Parkinson's (PD) and Huntington's disease

(HD). Repaglinide (REP) a meglitinides class drug is believed to act by targeting ATP-binding cassettes and stimulating the release of insulin from the β-cells of the pancreas [7]. REP exerted a neuroprotective effect against kainic acid-induced neuronal cell death in the CA3 region of hippocampal and rotenone-induced PD [8]. Further, recent studies have reported that REP exerted a strong neuroprotective effect in HD which may possibly work via multiple intracellular channel modulators, maintaining calcium homeostasis, gene expression, enzymatic activities, and targets neuronal calcium receptors by specifically attaching to them in a calcium-dependent manner. Recent evidence also indicated that REP down-regulates the expression of downstream regulatory element antagonist modulator (DREAM), (a calcium-binding protein) that regulates calcium homeostasis and is involved in the pathogenesis of HD and AD [8]. It has been reported that REP increases neuronal survival via upregulating the activating transcription factors-6 (ATF6) gene (endoplasmic stress sensor) that may possibly work via activating autophagy and inhibiting endoplasmic stress-induced apoptosis along with inhibition of the DREAM [9]. Thus, there is a huge possibility that REP regulates neurodegeneration via modulating the necrotic and apoptotic cell death protein expression of pro-apoptotic protein, anti-apoptotic protein, calcium homeostasis, and may eventually reduce neuronal cell death. This evidence clearly indicated the possible benefit of REP in DM and co-morbid conditions but the lack of strong evidence of its efficacy in AD.

Moreover, clinical reports suggest that repeated doses of REP need to be administered to exhibit pharmacological action as it has a poor pharmacokinetic profile, low solubility, low absorptivity, high protein binding, and substantial first-pass metabolism [7]. Therefore, to circumvent its pharmacokinetic properties and to improve its efficacy, the novel nanocarrier systems were designed with a targeted approach.

Nanocarrier systems have emerged as a promising strategy for targeted drug delivery, owing to their ability to overcome the limitations associated with conventional drug delivery approaches. These systems consist of nanoparticles, with sizes ranging from 10 to 1000 nm, which are designed to encapsulate and deliver therapeutic agents to specific sites in the body. Nanoparticles can be engineered with a variety of materials, including polymers, lipids, metals, and silica, to tailor their physicochemical properties, such as size, surface charge, and hydrophobicity, for optimal drug delivery[10].

Polymeric nanoparticles (PNPs) are one of the most extensively studied nanocarrier systems. They can be prepared by various methods, such as emulsion/solvent evaporation, nanoprecipitation, and electrospray, depending on the polymer type and desired nanoparticle properties. PNPs offer several advantages over other nanocarrier systems, such as

biocompatibility, biodegradability, and tunable drug release kinetics. In addition, they can be surface-modified with targeting moieties, such as antibodies, peptides, or aptamers, to enhance their specificity to diseased cells or tissues[11].

Furthermore, PNPs are often limited by their low drug loading capacity and susceptibility to aggregation, which can lead to reduced drug efficacy and toxicity. On the other hand, lipid-based nanocarriers can suffer from poor stability and limited versatility in drug delivery applications.

Therefore polymer-lipid hybrid nanoparticles (PLHNPs) have gained prominence due to their ability to combine the advantages of both polymeric and lipid-based nanoparticles for drug delivery applications. These nanoparticles are typically composed of a polymeric core and a lipid shell, and their unique structure offers several advantages over conventional drug delivery systems [12].

The polymeric core of PLHNPs provides high stability and robustness, allowing for prolonged circulation time in the bloodstream and protection of the drug payload from degradation. The lipid shell, on the other hand, provides a hydrophobic environment that facilitates the encapsulation of hydrophobic drugs, as well as the ability to interact with cell membranes for targeted delivery. At last, PLHNPs are a promising class of nanocarriers that combine the advantages of both polymeric and lipid-based nanoparticles for drug delivery. Their unique structure and ability to incorporate both hydrophobic and hydrophilic drugs, as well as functionalization with targeting ligands, make them attractive candidates for various biomedical applications [13].

Moreover, to enhance the pharmacokinetic and pharmacodynamic characteristics of nanocarriers, PEGylation has emerged as a facile and efficacious approach. It is a process of covalently attaching polyethylene glycol (PEG) polymer chains to nanocarrier systems such as liposomes, micelles, and nanoparticles. The surface of nanocarriers is typically coated with PEG, which can impart stealth properties by inhibiting protein adsorption and opsonization. This stealth effect helps nanocarriers evade the immune system and increases their circulation time in the bloodstream. PEGylation can also enhance the stability of nanocarriers and improve their ability to encapsulate hydrophobic drugs. It also improve the biodistribution and targeting of nanocarriers by modifying their surface charge and reducing their nonspecific interactions with biological tissues [14]. This feature allows for improved drug delivery to the target site and a reduction in off-target effects.

2. Objective: Based on the identified gaps in the existing research, the objective of the proposed research was categorized and prioritized into the areas that require further investigation and development.

Objective I : To evaluate the neuroprotective potential of REP in MetS associated with AD.

Objective II : To improve the efficacy and circumvent pharmacokinetic limitations of REP by developing brain targeted nano drug delivery system.

Objective III : To examine the best PEGylated nanocarrier system for targeting REP to the brain by oral route.

3. Materials & Methods:

3.1 Materials

3.1.1 Drugs and chemicals REP was provided by Tokyo Chemical Industry Co., Ltd. (Tokyo, Japan). FBS, DMEM, and penicillin–streptomycin solution was purchased from Gibco Life Technologies (U.S.A.). Phospholipon 90 H, soy lecithin, egg phosphatidylcholine, soy phosphatidylcholine, Distearoyl-sn-glycerol-3-phosphoethanolamine-Poly (ethylene glycol) (DSPE-PEG_{2000}) were provided by Lipoid. Poloxamer 407 was supplied by BASF (India). Porcine polar brain lipid (PBL) was acquired from Avanti polar. Dialysis tubing (10kDa) and Phosphate buffered saline; pH 7.4 (PBS) were obtained from Himedia (Mumbai, India). Insulin, Tumour Necrosis Factor alpha (TNF-α), and Interleukin-6 (IL-6) ELISA kits were procured from Ray Biotech Inc. Brain-Derived Neurotrophic Factor (BDNF) ELISA kit was purchased from Boster Biological Tech. Ltd, USA. Amyloid beta ($A\beta_{1-42}$) and phosphorylated tau protein (pTau) ELISA kits were acquired from Elab Science. Trizol reagent was purchased from Invitrogen, USA. SYBR green / ROX qPCR master mix kit was from Bio-Rad. Deionized ultra-pure water was obtained from the in-house Millipore Milli-Q Plus system with an electrical resistivity of 18.2 MΩ.cm (at 25˚C) (Millipore Bedford Corp., Bedford, MA, USA). The Primary and secondary antibodies like anti-Bax, anti-Bcl-2, anti-caspase-3, GAPDH, and anti-rabbit IgG antibody used in the present study were procured from cell signaling technology, Danvers, Massachusetts, USA. The ECL kit for visualization was a procedure from Thermo fisher scientific. Primers Activating transcription factor-6 (ATF-6) and GAPDH were purchased from Imperial Life Sciences limited.

3.1.2 *In vitro* Cell line: Human neuroblastoma SH-SY5Y cells were obtained from National Centre for Cell Science (NCCS), Pune, India. The cells were preserved in Dulbecco's modified Eagle's medium high glucose (DMEM-F12) comprising 20% (v/v) Fetal bovine serum (FBS),

and 1mL/L of antibiotic (Penicillin-streptomycin) media. The cells were incubated at 37 ±1°C with a 5% CO_2 humidified atmosphere in the incubator.

3.1.3 Animals The central animal facility, BITS-Pilani, Pilani campus, India (417/PO/ReBi/2001/CPCSEA) provided the wistar rats (200–220 g) for conducting the animal study. All animal experiments were accomplished as per Institutional Animal Ethic Committee (IAEC) guidelines of BITS-Pilani, Pilani campus, India (protocol number IAEC/RES/22/05/Rev-1/28/25). The animals were retained in polyacrylic cages under controlled conditions (12 h light/dark cycle, 22 ± 1°C with 60% relative humidity) and fed with the normal diet with purified water *ad libitum*.

3.2 Methods

3.2.1 *In vitro* experimental Procedure

3.2.1.1 Cell viability assay by MTT

The SHSY-5Y (P24) cells were cultured with 1.5×10^4 cells/well cell density [15]. After 24 h of seeding the cells were treated with test compounds at the concertation range of 0.25-100 µg/mL to screen out the effective concentration with time. Then cells were washed with sterile PBS solution in triplicate and 20 µL of MTT (5mg/mL) solution was added to form formazan crystals [16]. Further, culture grade DMSO (200 µL) was added to dissolve the crystals, and using a microplate spectrophotometer (Epoch, Biotek, Winooski, USA) the absorbance was measured at 570 nm, and 630 nm (reference wavelength).

3.2.1.2 STZ Treated neuroblastoma cell-based study

The assay was performed to understand the neuroprotective nature of test compounds on the SHSY-5Y cells induced with streptozotocin (STZ). Initially, the effective concentration of STZ was examined to originate metabolic stress into the cells[17]. The SHSY-5Y cells (3 X 10^4 cells/well) were seeded into 96 well plate and allowed to attach at 37 C in a 5% Co2 incubator. Further, the cells were treated with STZ at a concentration of 1-20 mM for 6 and 12 h to investigate the effective concentration and time[18]. Afterward, cells were treated with REP to estimate the cell viability and evaluate the protective effect of REP [19].

3.2.1.3 Reactive oxygen species-scavenging activity by hydrogen peroxide

The assay was performed to determine the intracellular ROS production, initially neuroblastoma SHSY-5Y cells were seeded into 96 well plate with a cell density of $15X10^3$ cells/well and allowed to be attached for 12 h at 37℃ in a 5% Co_2 incubator. Further cells were exposed to H_2O_2 at a concentration of 1-20 mM for 12 and 24 h to examine the effective

concentration and then treated with a test compound to evaluate the neuroprotective effect by estimating the percent cell viability [20].

3.2.1.4 Cellular uptake assay of nanoformulation

The SH-SY5Y (P29) cells were seeded on a glass coverslip with a cell density of 2×10^4 in the 6-well plate. The coumarin-6 (C6) loaded PNPs and PLHNPs (150 µL) were incubated with the cells in DMEM-F12 medium at 37 °C for 4 or 8 h. The cells were washed thrice with PBS (pH 7.4) and nuclei were counterstained with 4′,6-diamidino-2-phenylindole (DAPI, 1µg/mL, 30 min). Further, the cells were washed, resuspended in PBS, and mounted onto a glass slide after fixing with 4% paraformaldehyde solution and observed under a Carl ZEISS LSM 880 Axio confocal microscope (Jena, Germany). The quantitative estimation of cellular uptake was performed by flow cytometer. FACSAria SORP (Becton, Dickinson, San Jose, CA, USA) [21].

3.2.2 *In vivo* experimental Procedure

3.2.2.1 Induction of MetS and BIR linked with AD

The wistar rats (200-250 mg/kg) were acclimatized for seven days and afterward, diet manipulation was done with a High-fat diet (HFD) (Table 4.7). The HFD was fed for 16 weeks and then a low dose of STZ (30 mg/kg, *i.p)* was injected [22,23].

The wistar rats subjected to HFD with STZ exhibited characteristic features of IR were confirmed after 72 h of STZ administration and the assessment of body weight, fasting blood glucose level (FBGL), total cholesterol (TC), triglycerides (TG), glycosylated hemoglobin level (HbA1c), and insulin level were measured using commercially available kits. Fig. 3.1

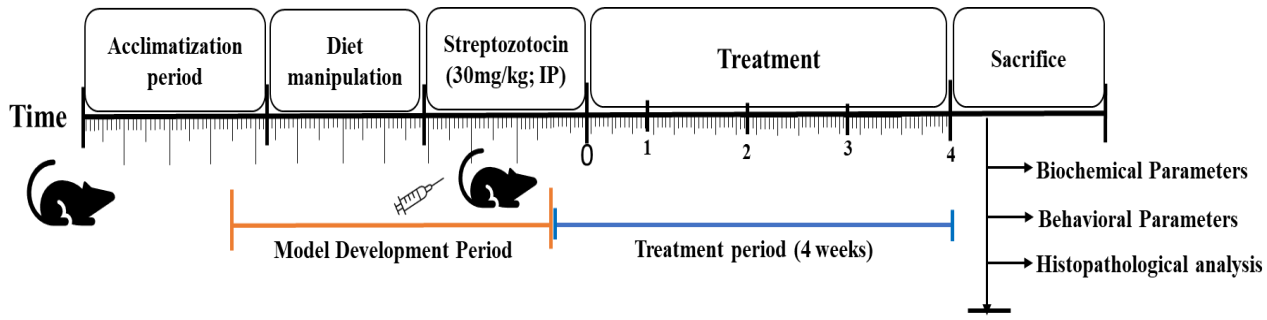

Fig.3.1: Experimental schedule of animal model development and treatment

3.2.2.2 Experimental Protocol for *in vivo* study

Initially, the animals were divided into four groups as in Table 3.1 to assess the neuroprotective effect of REP. The treatment was carried out for 4 weeks and biochemical parameters were examined and compared with an anti-Alzheimer drug as a standard.

Table 3.1: Experimental design for the screening of REP

Group 1	:	Normal pellet diet fed rats (Normal control)

Group 2	:	High-fat diet-streptozotocin diabetic rats (disease control), administer with Milli- Q water
Group 3	:	High-fat diet -streptozotocin-diabetic rats, administered with REP suspension (REP; 4mg/kg, *p.o*)
Group 4	:	High-fat diet -streptozotocin-diabetic rats, administered with memantine (MEM; 5mg/kg, *p.o*)
Group 5	:	High-fat diet -streptozotocin-diabetic rats, administered with PNPs; 4mg/kg, *p.o*
Group 6	:	High-fat diet -streptozotocin-diabetic rats, administered with PLHNPs; 4mg/kg, *p.o*
Group 7	:	High-fat diet -streptozotocin-diabetic rats, administered with REP suspension (4mg/kg, *p.o*) and MEM (5mg/kg, *p.o*)

The blood was collected from the retro-orbital plexus method. In brief, each wistar rat was hand restrained, the neck was gently scuffed and the eye was made to bulge then a glass capillary was inserted. The blood was allowed to flow by capillary action into the heparinized disposable tubes. The tubes were centrifuged at 7500 rpm for 20 min at 4 °C to separate out the plasma and stored at -80 ±10 °C [24,25]. Furthermore, serum metabolic parameters, neurochemicals biomarkers, Oxidative stress parameters, and proinflammatory cytokines were estimated.

3.2.2.3 Behavior assessment for cognitive and motor functions

(i) Passive avoidance task

The passive avoidance task was executed as per the previously described reports. In brief, the apparatus consists of an illuminated compartment and a dark compartment (Fig.4.3). Both compartments were separated by a guillotine door and equipped with a shock scrambler grid floor. Primarily, the acquisition trial was performed on each animal by placing them into the illuminated compartment for habituation of the 60s and after that, the guillotine door was opened to record the initial latency to enter the dark compartment. Animals with an initial latency period of more than 60s were excluded from further investigation. As the animal entered the dark compartment the guillotine door was closed and an electric foot shock of 50V, 50HZ, and 0.2mA was delivered for 3s through the foot grid. The animal was taken out from the dark chamber and returned to its cage. The retention latency was evaluated after 24h same as in the acquisition trial, but no foot shock was delivered. The latency time was measured up to 300s and chambers were cleaned and dried between the trials with 70% v/v alcohol [26].

(ii) Spatial navigation task

In the spatial navigation task, Morris Water Maze (MWM) comprised of a circular water tank (120 cm diameter, 60 cm height) filled with water (27±1 °C) to a depth of 40 cm and divided

into four equal quadrants such as south-west (SW), south-east (SE), north-east (NE) and north-west (NW). The escape platform (10 cm X 5 cm) was positioned in the center of one of the randomly selected quadrants; 2 cm below the water surface and remained in the same position throughout the entire experiment. Before the training phase, the animals were allowed to swim freely in the pool for 60 s without the platform. Animals were subjected to four trials per session for consecutive four days, with each trial having a time limit of the 60s. The animals remained on the hidden platform for the 30s after climbing onto it and before moving on to the next trial. In case animals failed to locate the hidden platform for the 60s, then were placed gently on the platform for 60s. Thereafter, the video tracking software Any-maze 7.1 was used to calculate the time required to locate the hidden platform [27].

(iii) Probe trial

The escape platform (10 cm X 5 cm) was positioned in the center of the randomly selected quadrants of the pool below 2 cm to the water surface and kept in the same position throughout the entire experiment (south-east for this study) (Fig. 5.9). The animals were permitted to swim freely into the pool for 60 s without a platform before the training started. Animals received a training session consisting of 4 trials per session (once from each starting point) for 4 days, each trial having a ceiling time of 60s. After climbing onto the hidden platform, the animals remained there for 30 s before commencement of the next trial. If the animal failed to locate the hidden platform within the maximum time of 60 s, it was gently placed on the platform and allowed to remain there for the same interval of time. The time taken to locate the hidden platform (latency in seconds) was calculated using ANY-maze video tracking system (Stoelting, USA).

(iv) Novel object recognition

The rodent's ability to recognize the new object in their environment was assessed by novel object recognition (NOR) task. The NOR task consists of three stages habituation, familiarization, and test stage. In habituation phase, the animals have free access to explore the open field arena for 5 min in the absence of an object on two consecutive days. In familiarization phase, two identical sample objects were placed in the open field arena and animals were placed for the 5min. Whereas during the test phase (24 h later to familiarization phase), the two objects; one identical to the sample and another novel object were placed in the open-filed arena [28]. The objects were placed in the opposite and symmetrical corners of the arena during the familiarization and test phase and time spent was recorded for 5 min to explore the novel or familiar object. The task was performed by using ANY- maze 7.1 software.

3.2.2.4 Molecular studies

3.2.2.4.1 Quantitative Real-time Polymerase Chain Reaction (qRT-PCR)

Total RNA from the rat's brain tissue sample was isolated with the TRIzol reagent, according to the manufacturer's protocol. Further RNA was reverse transcribed to complementary DNA (cDNA) by using a Revert Aid First strand cDNA synthesis kit [29]. Moreover, the SYBR green / ROX qPCR master mix kit was used for amplification according to the manufacturer's procedure using the CFX connect Optics Module by Bio-Rad[30]. The PCR conditions for the transcription level of ATF6 were 98℃ for 8 min followed by 32 cycles at 94℃ for 25 sec, 50℃ for 35 sec and 72℃ for 1 min. The relative expression level of activating transcription factor 6 (ATF6) mRNA was calculated keeping glyceraldehyde-3-phosphate dehydrogenase (GAPDH) as a housekeeping gene and determined by the $2^{-\Delta\Delta t}$ method[31].

3.2.2.4.2 Western blot analysis

The total proteins from the hippocampal region of the brain were extracted in a RIPA lysis buffer supplemented with protease, trypsin, and phosphatase inhibitors. Further, the amount of protein in the sample was detected using a BCA protein assay[30,32]. The collected lysate was separated using 12% SDS-PAGE gel using the electrophoresis technique and then transferred onto the PVDF membrane[33]. The blots were probed overnight with anti-bodies anti-Bax, anti-Bcl-2, ant-caspase-3, and GAPDH at 4℃. Further, a secondary antibody (anti-rabbit IgG antibody) was used and signals were visualized using an ECL kit.

3.2.2.4.5 Assessment of histological changes

In histopathological analysis, brain samples were harvested immediately and fixed with formalin solution (10% V/V). Then samples were embedded into paraffin wax and sectioning them to 5 µm sections. The prepared sections were stained with hematoxylin and eosin stain (H&E) and hippocampal regions (dentate gyrus and cornu ammonis) were examined under the Zeiss microscope. The deteriorating neurons were evaluated in terms of percentage by using ImageJ software.

3.2.3 Pharmacokinetic profile

The pharmacokinetic study was performed in wistar rats (200-250g) to measure the pharmacokinetic parameters of REP and nanocarrier system. The rats were acclimatized for 7 days and prior to the study and rats (n=4) were fasted overnight. Then REP was administered at a dose of 4 mg/kg, *p.o* with the dosing volume of 1 mL to each overnight fasted rat, and blood was collected in heparinized disposable tubes from retro-orbital plexus at pre-set time intervals. Moreover, the blood was centrifuged at 7500 rpm for 20 min to separate out the plasma and stored at -80 ±10 °C for further analysis [24,25]. The plasma concentration-time profile

was plotted, and the pharmacokinetic parameters were investigated by Phoenix Win Nolin Certera^{TM} (Pharsight, U.S.A; version 8.0) with non-compartmental modeling.

3.2.4 Biodistribution

The biodistribution of REP and nanocarrier systems was investigated in the wistar rat, the animals were anesthetized (ketamine/ xylene) and sacrificed at predetermined time intervals (0.25h, 2h, 6h, 12h, and 24 h four rats/time point) by cervical dislocation. Further, the highly perforated organs (brain, and liver) were collected promptly and thoroughly rinsed in ice-cold saline to remove blood, and other content and blotted dry with filter paper [34]. Further, the samples were prepared and analyzed with an in-house developed bioanalytical method.

3.2.5 Development and optimization of Formulations

3.2.5.1 Synthesis and characterization of di-block amphiphilic polymer:

The di-block polymer was synthesized by a ring-opening method. The m-PEG (M ~ 5000 Da) was dissolved in toluene, and ε-caprolactone was added dropwise. Afterward, tin (II) 2-ethyl hexanoate was mixed, and the reaction was processed under a nitrogen atmosphere at 110 ◦C for 24 h [26]. Further, the reaction mixture was concentrated using a rotary evaporator, and the product was dissolved in dichloromethane, then chilled methanol was added to the obtained precipitate. Later wash the precipitate thrice with chilled diethyl ether and dry it properly (Fig.3.2) [27]. The synthesized polymer was evaluated and characterized by 1H NMR and by gel permeation chromatography (GPC).

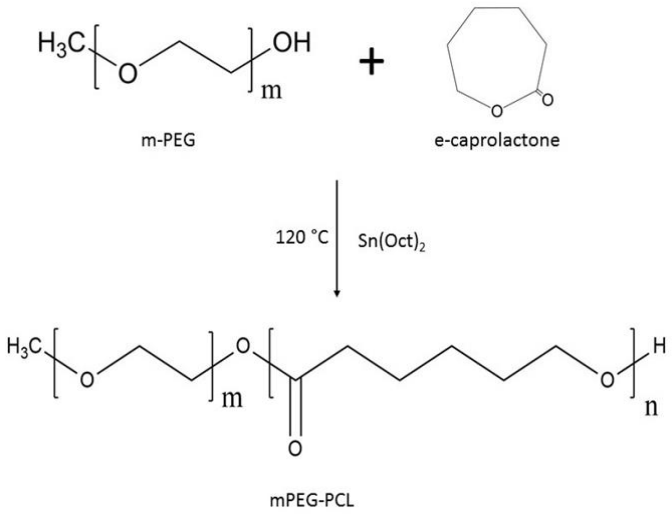

Fig. 3.2: Schematic representation of polymer synthesis

3.2.5.2 Fabrication of polymeric nanoparticles (PNPs)

The polymeric nanoparticles were formulated by the nanoprecipitation technique with modifications[35]. In brief, 2.5mg of REP, mPEG-PCL polymer was dissolved in 2 mL of

acetonitrile (ACN) (Organic phase) followed by dropwise addition of 10 mL poloxamer 407 solutions (aqueous phase) under magnetic stirring for 3 h at 37℃ [35] (Fig. 3.3).

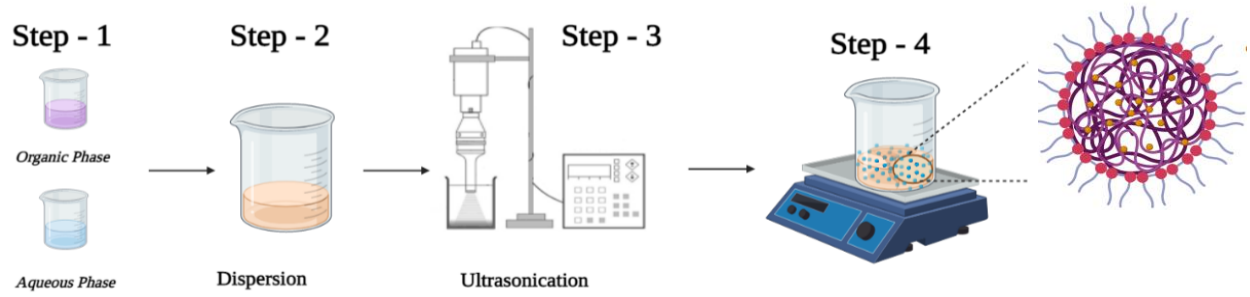

Fig.3.3: Schematic representation of PNPs preparation procedure

The remaining amount of organic solvent was removed using a rotary evaporator and analyzed by headspace-gas chromatography (HS-GC).

3.2.5.3 Fabrication of Polymeric lipid-hybrid nanoparticles (PLHNPs)

The PLHNPs were fabricated by a one-step self-assembly method.[36] In brief, a lipid monolayer was prepared by phospholipid, and DSPE-PEG 2000 after dissolving in a 4% v/v ethanol-water solution. Further, the lipid solution was added dropwise into the deionized water containing 1% w/v stabilizer at 65℃ to maintain the dissolution situation of both the lipids and prepared an aqueous lipid dispersion medium. Additionally, the weighed amount of REP (1 mg) and poly lactic-co-glycolic acid (PLGA,10mg) were dissolved in the acetonitrile (ACN). The organic phase containing drug and polymer was poured dropwise into the aqueous lipid dispersion medium (phospholipid, DSPE-PEG 2000, stabilizer) under probe sonication followed by continuously stirring at 400 rpm for 3 h and allowed to self-assemble.[13,37] Further, the rotary evaporate was used to remove the organic solvent residue in the PLHNPs and analyzed by headspace-gas chromatography (HS-GC) (Fig.3.4)

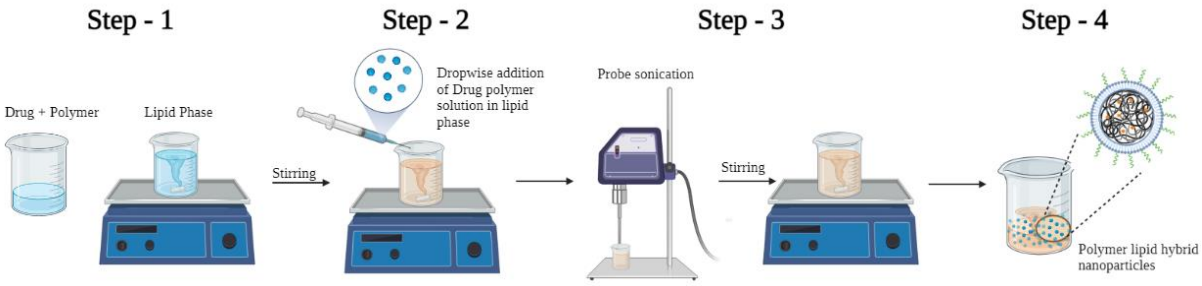

Fig.3.4: Schematic representation of PLHNPs preparation procedure

3.2.5.4 Optimization of formulation using quality by design approach

(i) Quality Target Product Profile (QTPP)

A QTPP assists in predicting the essential characteristics of the drug product that can be attained to ensure the safety, quality, and efficacy of the drug product. QTPPs are the pivotal elements of the QbD approach and have a crucial role in defining the objectives to develop the drug products (Table.4.13).

Table.3.2: Quality target product profile (QTPP) of REP-loaded PNPs and PLHNPs

Target Product Profile	Target	Justification
Dosage	Powder	For ease oral application
Route of administration	Oral	Patient compliance
Appearance	White	Flowable and odorless
Particle size	<150 nm	Enhance permeation to BBB
PDI	< 0.5	Uniform distribution of particle size
Entrapment efficiency	Maximum with desired size range	Maximum entrapment improves permeation and increases drug loading
Release	Control release compared to free drug	Prolong the effect and enhance the efficacy

(ii) Initial risk assessment

Initial risk assessment assists in recognizing the material attributes and process parameters which effectively affect the product CQAs. Based on the initial experimental data and prior knowledge, a risk assessment tool could be used to identify the order and rank of parameters that could potentially impact the quality of the final product. Initially, the interdependence rating was executed on a three-level scale between CQAs, CMAs, and CPPs and categorized as “high” (H), “medium,” (M), or “low” (L). Afterward, a rating was performed related to the selected CQAs, CMAs, and CPPs, and risk estimation results were calculated and ranked according to severity scores (Table.3.3) [38].

Table.3.3: Risk estimation matrix (REM) for initial risk assessment of different material attributes and process parameters by qualitative analysis.

Critical quality attribute	Material attributes and process parameters Polymeric nanoparticles (PNPs)						
	Drug polymer ratio	Amount of stabilizer	Stirring speed	Stirring time	Organic solvent	Sonication time	Sonication amplitude
Particle size	High	High	High	Medium	Low	High	High
PDI	High	Medium	High	Medium	Low	Medium	Medium
Entrapment efficiency	High	High	Medium	High	High	High	Medium
	Polymer lipid hybrid nanoparticles (PLHNPs)						

	Drug polymer ratio	Lipid polymer ratio	Lipid DSPC-PEG_{2K} ratio	Amount of stabilizer	Stirring time	Stirring speed	Sonication time
Particle size	High	High	Medium	High	Medium	High	High
PDI	High	Medium	Low	Medium	Medium	High	Medium
Entrapment efficiency	High	High	High	High	High	Medium	High

(iii) Optimization of data analysis and model validation

The optimization of data analysis and model validation was done by Design Expert® software 13. The interaction of the factors was assessed by the second-order polynomial (quadratic) equation which is created by the experimental design

$$Y=b0+b_1A+b_2B+b_3C+b_{12}AB+b_{13}AC+b_{23}BC+b_{11}A^2+b_{22}B^2+b_{33}C^2$$

Here Y denotes response; b_0 indicates constant; b_1, b_2, and b_3 represent linear coefficients, b_{11}, b_{22}, and b_{33} are quadratic coefficients, and b_{12}, b_{13} b_{23} signify interaction coefficients. Further A, B, and C represent the coded intensity of independent variables. The terms A^2, B^2, and C^2 define the interaction and quadratic terms, respectively. The fit of data was evaluated by the factor-response relationship in terms of analysis of variance (ANOVA), lack of fit, coefficient of correlation (R^2), adjusted R^2 (R^2-adj), and predictive R^2 (R^2-pred). The regression model fitted well when the lack of fit is $P < 0.05$ (lower than the pure error), but the model is attuned poorly when the lack of fit is $P > 0.05$ (lower than pure error). Furthermore, the factor-response relationships were computed and depicted graphically via 2D-contour plots and 3D-response surface plots [38].

3.2.6 Physicochemical characterization

(i) Particle size, Poly dispersibility index, and Zeta potential: Dynamic light scattering (DLS) method was used to measure the z-average PS, PDI, and zeta potential (ZP) of the formulated PNPs and PLHNPs using a Malvern Nano ZS (Malvern Instruments Ltd., UK). The prepared nano-dispersion was diluted in a ratio of 1:10 with filtered milli-Q water and sample analysis was carried out at 25˚C, 173˚backscattering with 1.330 dispersants refractive index for determination of PS, PDI.

(ii) Entrapment efficiency (EE): The EE of PNPs and PLHNPs was determined by the ultracentrifugation technique. The dispersant was centrifuged at 40,000 RPM for 35 min at 10 ˚C after this the centrifuged pellet was diluted with ACN, and bath sonicate for 15 min. The samples were examined by the RP-HPLC method and EE was calculated by using the below-mentioned formula.

$$EE\% = \frac{Amount\ of\ REP\ in\ nanocarrier}{Theortical\ amount\ of\ REP\ loaded\ during\ preparation} \times 100$$

(iii) Morphological characterization: The surface morphological characterization of PNPs and PLHNPs was determined by field emission-scanning electron microscopy (FE-SEM) and high-resolution transmission electron microscopy (HR-TEM). In FE-SEM the nano dispersion of PNPs and PLHNPs (500µL) were diluted in Milli Q water and dried samples were positioned on carbon tape affixed to a metal stub and sputtering was done with gold for the 90s using a Quorum Technologies Q150TES sputter coater (East Sussex, England) to avoid charge accumulation. Further, coated nanoparticles were examined by an FE-scanning electron microscope (Hillsboro, Washington) at 20,000× magnification, 20 kV high vacuum, a spot size of 9.0, and a scale of 0.2−3 µm. Moreover, in HR-TEM analysis (Hitachi (H-7500) the nano dispersion of PNPs and PLHNPs have splayed on a carbon-coated copper grid and was stained for visualizing with 2% urinyl acetate.

(iv) *In vitro* drug release study

In vitro release study of REP, PNPs, and PLHNPs were carried out by using the dialysis bag method. REP, PNPs, and PLHNPs (equivalent to 500 µg of REP, n=3) were inserted into an overnight dipped dialysis bag (MWCO of 10 kDa, Himedia Laboratories. Pvt. Ltd.,). The bag was sealed from the sides with the thread and dipped in 50 mL of biorelevant dissolution media (phosphate buffer saline, pH 7.4 containing 0.1% sodium dodecyl sulphate) under a shaking water bath (120 rpm, 37 ± 0.5 °C).[39] The 1mL aliquot of the release media was withdrawn at preset intervals and replenished with the same volume. Further, samples were filtered and analyzed by the RP-HPLC method.[35] The drug release mechanism and kinetic were calculated by mathematical models using a DD solver (an Excel add-in). The best-fit model of the release profile was determined based on the lowest Akaike index criteria (AIC) value and high regression coefficient (R^2).

(v) Stability in simulated biological fluids

The stability of PNPs and PLHNPs in a simulated gastrointestinal tract (GIT) was investigated by three phases mouth phase, gastric phase, and intestinal phase. In order to mimic the conditions, all the solutions and/or samples were pre-incubated in a bath shaker at 37˚C at 100 rpm. Simulated saliva fluid (SSF) was prepared by using 30 mg/mL mucin and other salts to modulate the mouth phase conditions. The PNPs and PLHNPs were associated with SSF at a mass ratio of 1:1 and the mixture were placed in a bath shaker for 10 min with adjusted pH of 6.8. Whereas in the gastric phase, simulated gastric fluid (SGF) consisted of 3.2 mg/mL pepsin, 0.1mM hydrogen chloride, and 2 mg/mL sodium chloride. The sample was taken from the

mouth phase and mixed with the SGF at a mass ratio of 1:1 and the mixture was placed in a bath shaker for 2 h.[40] In intestinal Phase, the sample was taken from the gastric phase and diluted in a mass ratio of 1:1 with simulated intestinal fluid (SIF) which is composed of 0.5M CaCl2, 7.5 M NaCl, 50mg/mL bile extract, and 24 mg/mL pancreatin. The mixture was placed in a bath shaker for a further 2h to mimic the conditions (Fig.3.5) [41].

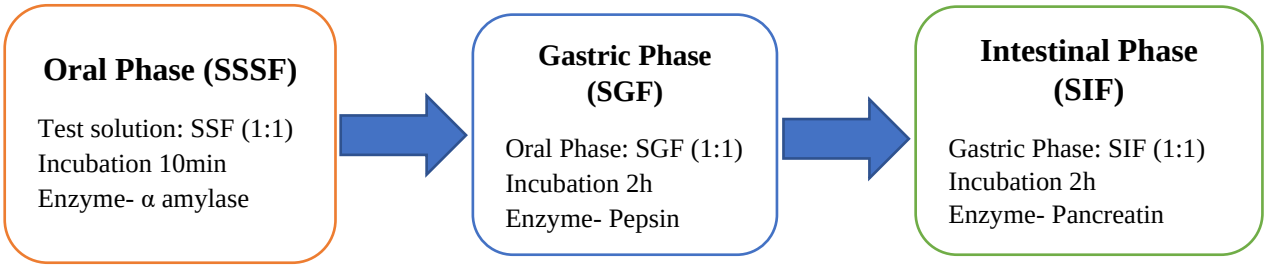

Fig.3.5: The flowchart to perform Gastro-intestinal stability studies

3.2.7 *In situ* absorption and permeation assay

(i) Single pass intestinal perfusion (SPIP) model

The animals were retained in polyacrylic cages under controlled conditions (12 h light/dark cycle, 22 ± 1°C with 60% relative humidity) and fed with the normal diet with purified water *ad libitum*. The wistar rats were acclimatized for at least seven days and then divided randomly into groups *viz.* REP, PNPs, and PLHNPs. Furthermore, rats were fasted for approximately 12-16 h, with free access to water, and anesthetized by intraperitoneal administration of xylazine (0.02g/kg) and ketamine (0.10g/kg). The rats were laid on a heating pad or kept under the lamp to maintain a body temperature of 37 ± 1˚C[42,43]. Afterward, the laparotomy was performed, through a middle incision of approximately 4 cm in the abdomen to isolate the proximal jejunum portion (15-20 cm) of the small intestine (Fig.3.6). Furthermore, the proximal jejunum area was cannulated from both ends by using a plastic tubing of 3 mm o.d [12].

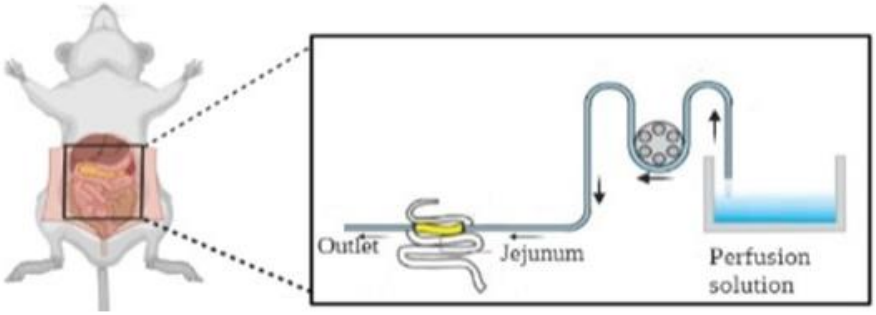

Fig.3.6: Illustration of SPIP model for in situ permeation study in wistar rat model.

The intestinal segment was gently washed with prewarmed (37±1℃) blank perfusion solution (Table.4.16) for nearly 30-45 min at a 0.5 mL/min flow rate or until the solution was clear.

Thereafter, the perfusion solution containing REP/ PNPs/PLHNPs was infused for 1 h (approximately) with a 0.2 ml/min flow rate to achieve a steady state or equilibrium state with the intestinal membrane [44]. As it reached a steady state, the perfusion solution was collected at the pre-determined time interval of every 15 min and withdrawn samples were immediately frozen at -80°C until further analysis [44–47].

(ii) Parallel artificial membrane permeability assay-blood brain barrier (PAMPA-BBB)

The PAMPA assay was mainly conducted to investigate passive permeability. In brief, samples were prepared at the concentration of 1.0 mM in dimethyl sulfoxide (DMSO) and diluted with Phosphate Buffer Saline (PBS); at pH 7.4 to make secondary dilutions for the donor compartment. Further, the filter membrane was layered with porcine polar brain lipid (PBL, 5 µL) extract solution and the receiver well contained 400 µl PBS. Consequently, the plates were placed over each other as a sandwich where the PBL-coated membrane was positioned between and maintained to prevent the formation of air bubbles at the lower side (Fig.3.7). Then the plate was incubated without agitation for 18h at room temperature [48,49]. Furthermore, the samples were collected from the donor and acceptor compartment, diluted adequately, and quantified by the RP-HPLC method. The assay was carried out in triplicates and the permeability coefficient (Pe) was estimated[50].

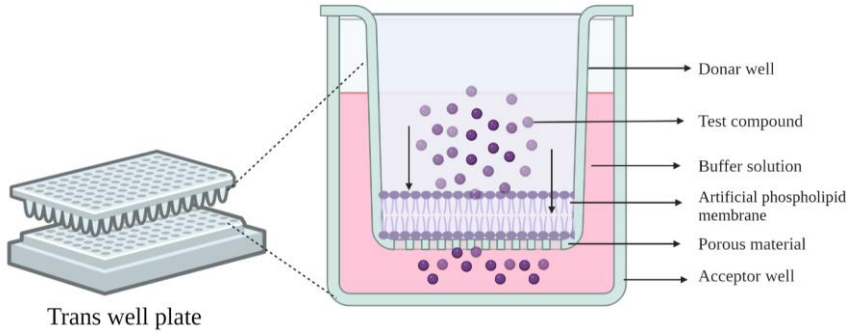

Fig.3.7: Illustration of Parallel artificial membrane permeability assay-blood brain barrier (PAMPA-BBB)

3.2.8 *In vitro* & *In vivo* analysis

The *in vitro* cell culture-based studies (cell viability, cell uptake, STZ and hydrogen peroxide assays) and *in vivo* (pharmacodynamic, pharmacokinetic and biodistribution) studies were performed as mentioned in the above sections 3.2.1 and 3.2.2 respectively.

3.2.9 Data analysis

All results were expressed as mean ± standard error mean (S.EM.). The experimental data were analyzed using a graph pad with a one-way analysis of variance (ANOVA) followed by Tukey's test at a defined significant level of $p < 0.05$.

4. Result & Discussion:

4.1 *In vitro* studies on neuroblastoma cell lines (SHSY-5Y)

4.1.1 Cell viability assay

The viability assay indicates the number of live and/or healthy cells in a sample and measures the physical or cellular health in response to chemical agents, therapeutic treatments, or extracellular stimuli is referred to as cell viability assay. Here, cell viability was estimated by MTT assay in which oxidative metabolic activates were measured based on NAD(P)H-dependent dehydrogenase enzyme activity. Primarily, the concentration of REP (0.25-100 µg/mL) was explored on SHSY-5Y cells, and a dose or concentration-dependent toxicity was observed as shown in Fig.4.1. Therefore, the results suggested that at 1 µg/mL around ~80-85% cells were viable, which was used for further analysis.

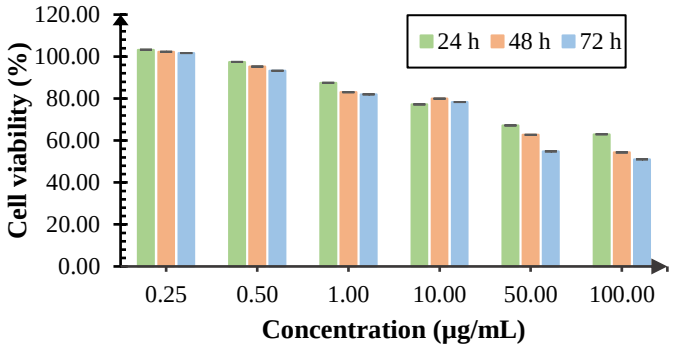

Fig.4.1: Cell viability assay of REP on neuroblastoma SH-SY5Y cell line.

4.1.2 STZ Treated neuroblastoma cell-based study

STZ is a diabetogenic agent which accelerated brain aging, hippocampal atrophy, Aβ aggregation, and loss of synaptic connections [15]. In neurons, STZ leads to depolarization of the mitochondrial membrane, oxidative stress, increase apoptosis, tau protein phosphorylation, and decrease glucose uptake [51]. Thus, to understand the effect of REP on STZ-treated cells the concentration of STZ was screened out from 1 mM to 20 mM. The concentration-dependent response was observed at 2.5 mM STZ for 12 h and the viability of cells was observed around 60-65% (Fig.4.2). Further, the STZ-induced SHSY-5Y cells were incubated with REP and an increment of around 1.2 folds in the cell viability of the cells was observed which represents a significant ($p<0.01$) effect on STZ-induced cells. Though the improvement in cell viability represents an effective potential of REP for neurodegenerative disorders.

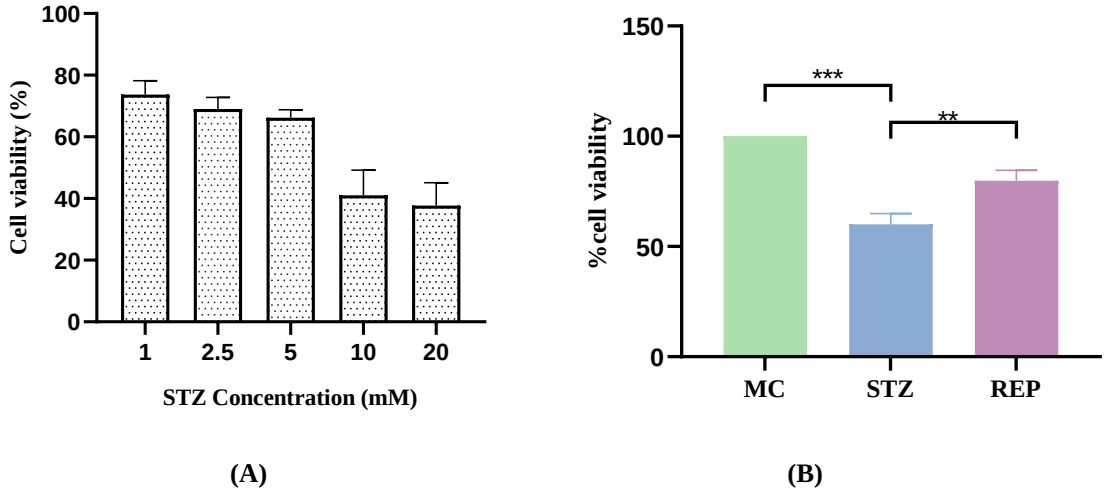

(A) **(B)**

Fig.4.2: (A) Screening of STZ concentration; (B) The effect of REP on STZ-treated SHSY-5Y neuroblastoma cell lines. and ** Indicates *P< 0.01, *** P< 0.001* by one-way ANOVA followed by Tukey's post hoc multiple comparison test

4.1.3 Reactive oxygen species-scavenging activity by hydrogen peroxide

H_2O_2 is an oxidizing agent which causes cellular damage and halts cell cycle development, resulting in cell death. The optimal H_2O_2 concentration for inducing cell death was determined by performing the preliminary studies in which 0.5-20mM concentrations were screened and observed that at higher concentrations, maximum cells were detached from the surface and float in the media (Fig.4.3). Whereas at low concentrations the viability of cells was around 80-85 % in 24 h. However, at a concentration of 1mM, the viability of cells was observed 70-75% in 24 h but in 12 h the viability reduced and showed around 60% viability. Thus, 1mM concentration of H_2O_2 was selected for further analysis. Afterward, the H_2O_2-treated SH-SY5Ycells (1mM, 12h) were incubated with REP and the study indicates that the REP represents around1.3-folds increment in cell viability and showed a significant ($p<0.01$) effect on H_2O_2 treated cells.

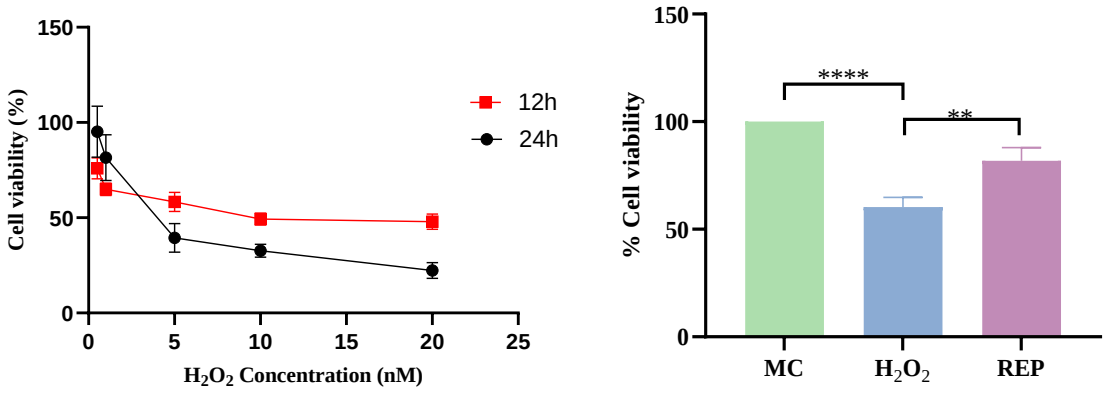

(A) **(B)**

Fig.4.3: (A) Screening of H_2O_2 concentration and (B) neuroprotective effect of REP on H_2O_2 treated SH-SY5Y neuroblastoma cell lines

4.2 *In vivo* studies

4.2.1 Estimation of Neurochemicals bio markers

Biomarkers are an integral part of drug development and help to measure the effectiveness of an investigational drug. However, it has been well reported that Aβ deposition, hyperphosphorylation of tau proteins, and reduction in the level of BDNF are the characteristic features of neurodegeneration and play a key role in AD pathogenesis. Thus, the effect of REP on neurochemical parameters (BDNF, Aβ, and tau protein) was estimated in HFD+STZ-induced wistar rats after the 4 weeks of treatment (Fig.5.13). It was observed that the DC group rats showed a significant ($p<0.001$) upregulation in the levels of Aβ and tau proteins than the NC group rats. Whereas the BDNF level was significantly ($p<0.001$) reduced in DC group rats than the NC group. Therefore, after treatment with REP for 4 weeks a significant ($p<0.01$) reduction in the level of Aβ and tau proteins was observed as shown in Fig.4.4 (A &B). Whereas the level of BDNF was improved significantly ($p<0.01$) compared to DC group rats. Moreover, significant ($p<0.01$) changes in the level of Aβ, tau proteins, and BDNF were also observed compared to MEM. Thus, the observed results suggest that the REP also has the ability to act as a neuroprotective agent and helps in the treatment of various neurodegenerative disorders.

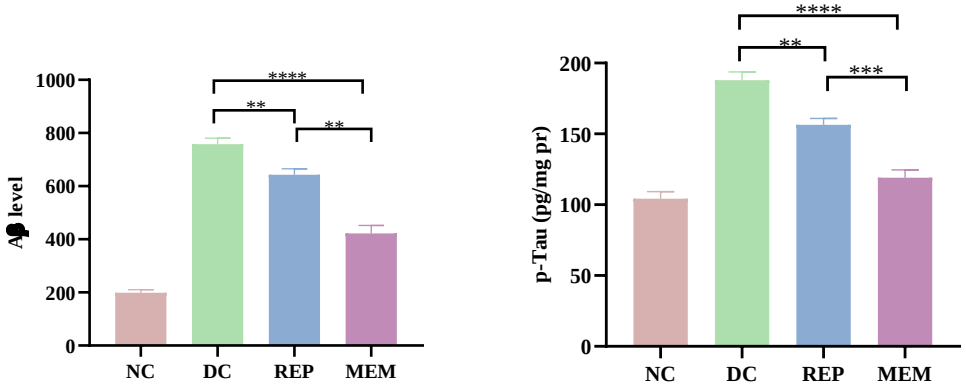

(A) **(B)**

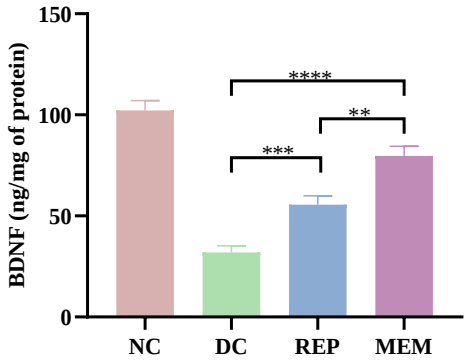

(C)

Fig.4.4: *In vivo* estimation of neurochemical parameters to understand the effect of REP after the treatment (A) Aβ level; (B) p-Tau; and (C) BDNF; in brain homogenate of HFD+STZ induced wistar rats, data are represented in (mean ± SEM, n=6 rats per group). * Indicates *P< 0.05; ** P< 0.01, *** P< 0.001, **** P< 0.0001* by one-way ANOVA followed by Tukey's post hoc multiple comparison test

4.2.2 Estimation of Proinflammatory cytokines

The level of inflammatory cytokines (TNF-α and IL-6) were observed (Fig.4.5) and found a significant (*p<0.0001*) upregulation in the DC group compared to NC rats. After the treatment with REP, a decrement in these levels was observed and showed a significant (*p<0.001*) suppression as compared to DC. Likewise, the REP showed a significant (*P<0.05*) change in TNF-α and IL-6 levels compared to MEM.

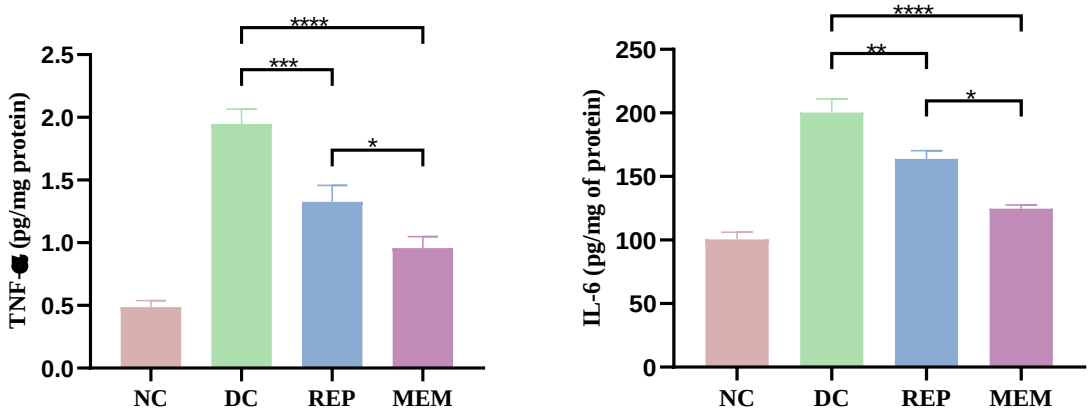

(A) **(B)**

Fig.4.5.: *In vivo* estimation of proinflammatory cytokines to understand the effect of REP on (A) TNF-α; (B) IL-6 level in brain homogenate of HFD+STZ induced wistar rats, data are represented in (mean ± SEM, n=6 rats per group). * Indicates *P< 0.05; ** P< 0.01, *** P< 0.001, **** P< 0.0001* by one-way ANOVA followed by Tukey's post hoc multiple comparison test

4.2.3 Estimation of Oxidative stress parameters

In this study, the level of GSH, SOD (antioxidant) MDA, and nitrite (oxidative markers) were determined to understand the role of REP. ROS generation (oxidative stress) plays a significant

effect in the production of neurodegeneration. The hippocampus and neocortex regions of the brain were the most vulnerable to oxidative stress-induced impairment. Therefore, the effect of REP on these parameters was measured and results showed that DC group rats significantly (*p<0.001*) increase the levels of oxidative markers i.e., MDA and nitrile, and decreased the levels of endogenous antioxidants i.e., GSH, and SOD compared to NC group as shown in Fig.4.6 However, after the treatment with REP the reduction in the level of MDA and nitrile was observed compared to DC. Moreover, REP significantly resulted in the attenuation of oxidative markers (GSH &SOD) in comparison to DC.

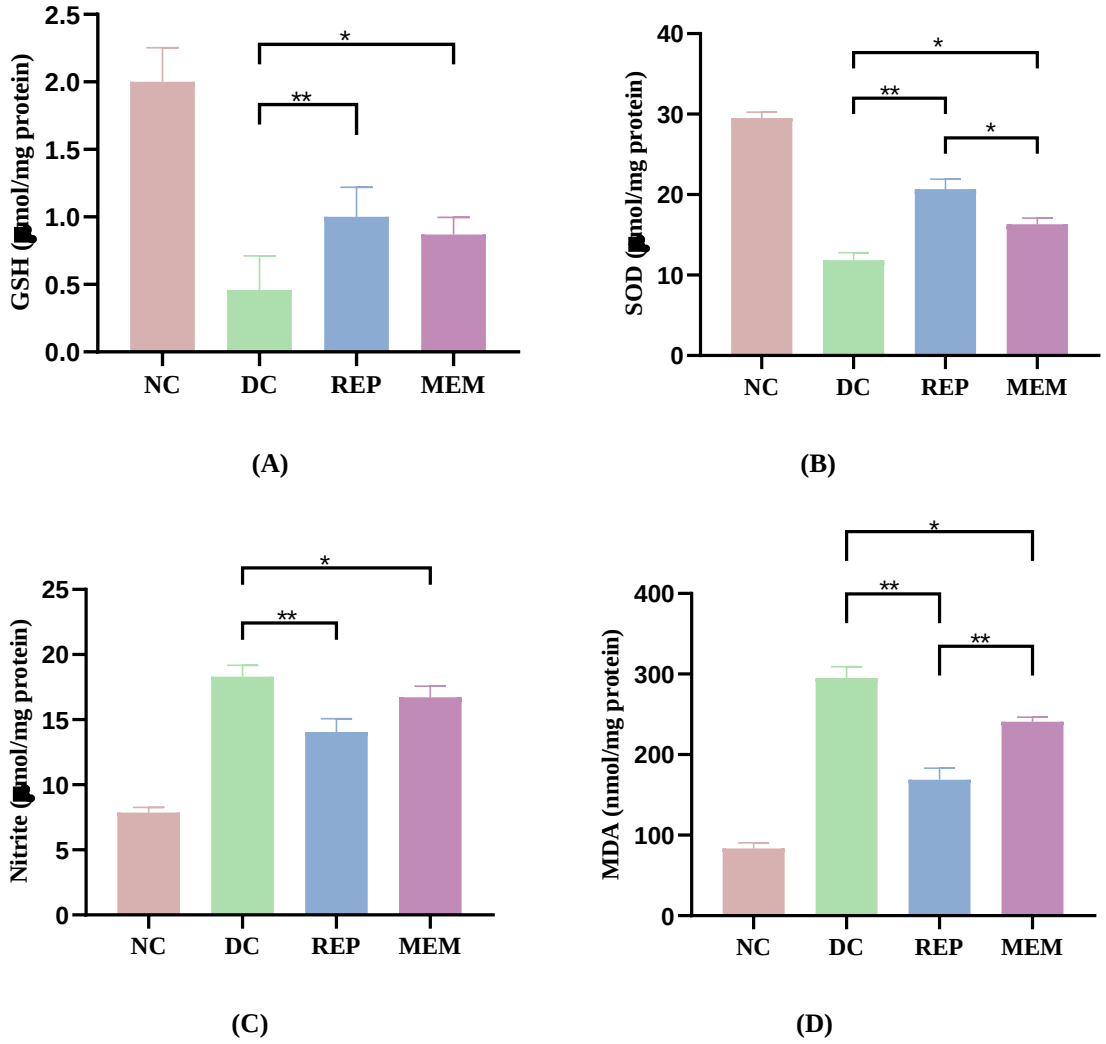

Fig.4.6: *In vivo* estimation of proinflammatory cytokines to understand the effect of REP on (A) GSH; (B) SOD; (C) Nitrite; (D) MDA level in brain homogenate of HFD+STZ induced wistar rats, data are represented in (mean ± SEM, n=6 rats per group). * Indicates *P< 0.05;* ** *P< 0.01*, *** *P< 0.001*, **** *P< 0.0001* by one-way ANOVA followed by Tukey's post hoc multiple comparison test

4.2.4 Behavior assessment by cognitive and motor functions

4.2.4.1 Passive avoidance task

A task in which rodents learn to abstain from a response to avoid the aversive stimulus. The test is used to evaluate the learning and memory in cognitive dysfunctions of the central nervous system. During the acquisition trial, no significant *(P>0.05)* differences in the initial latency time of all the groups were observed. Whereas in retention latency (after 24h of acquisition trial) analysis a significant *(P<0.01)* decreased in latency was observed in the HFD+STZ group as compared with NPD (NC) group (Fig.4.7). However, rats treated with REP showed a significant (*P<0.01*) amelioration in the retention latency compared to the DC group which showed improvement in retention memory.

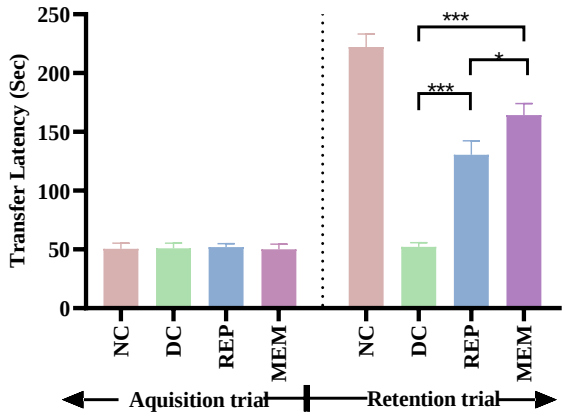

Fig. 4.7: Estimation of transfer latency by performing behavioral parameters using passive avoidance task. Data are represented in (mean ± SEM, n=6 rats per group). * Indicates *P< 0.05;* *** *P< 0.001*, by one-way ANOVA followed by Tukey's post hoc multiple comparison test

4.2.4.2 Morris Water maze (MWM)

After four days of training, the mean escape latency in all groups decreased gradually in MWM analysis. However, in the DC group, the mean escape latency was significantly higher in comparison with the NC group. Though there was a significant decrease in escape latency after treatment with REP and attenuated the effect compared to DC, as shown in Fig.4.8. After the hidden platform was removed in the probe trial test, it was found that DC group rats were unable to identify the exact location of the platform and spent less time in that quadrant than the NC group rats. Further, REP was administered for 4 weeks, and it was observed that REP group rats spent more time in the platform quadrant than the DC group rats, indicating that the REP improved the spatial and learning memory. These findings indicate that REP can help to reduce cognitive behavior in rats.

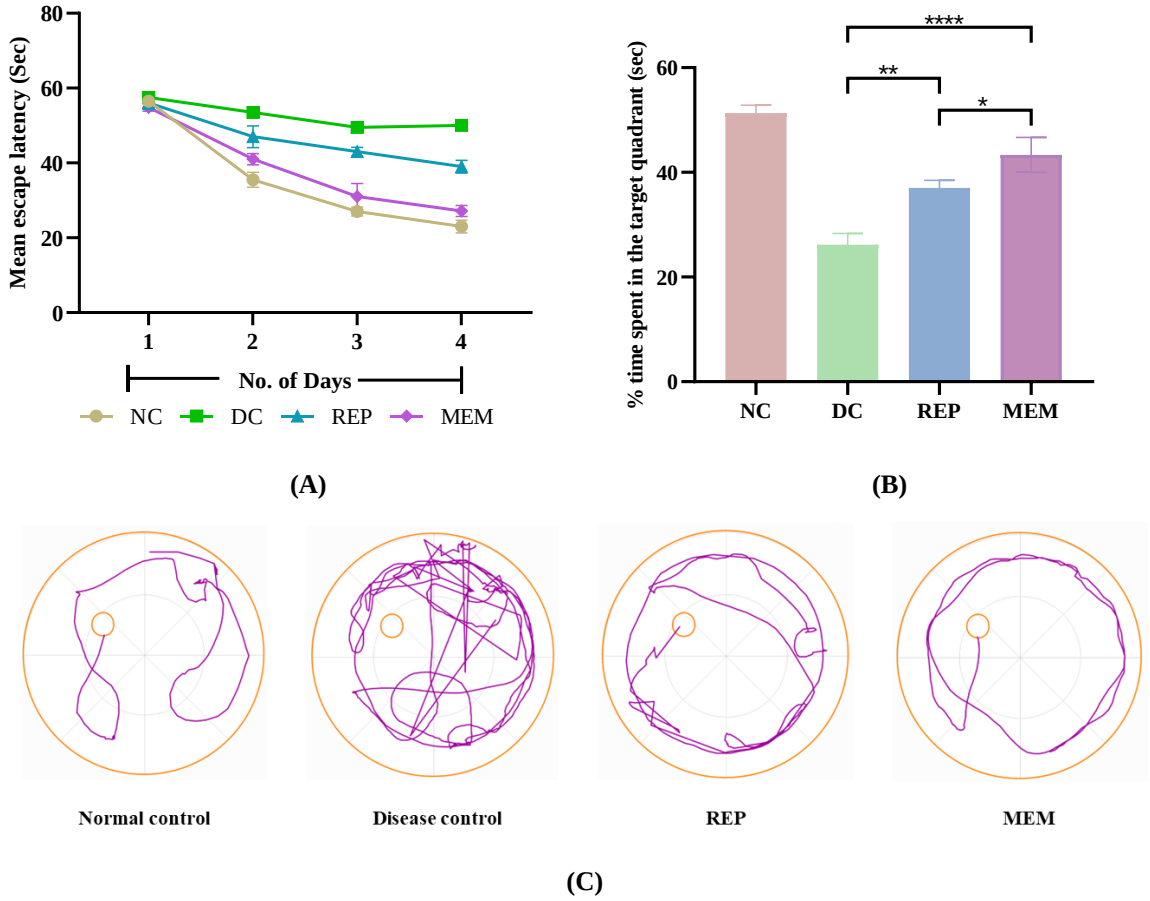

Fig.4.8: Estimation of (A) mean escape latency, (B) time spent in the same quadrant, and (C) representation of track plot for Morri's water maze task. Data are represented in (mean ± SEM, n=6 rats per group). * Indicates *P< 0.05; ** P< 0.01, **** P< 0.0001* by one-way ANOVA followed by Tukey's post hoc multiple comparison test

4.2.3 Molecular Studies

4.2.3.1 Quantitative Real-time Polymerase Chain Reaction (qRT-PCR)

The effect of REP was evaluated on the expression of ATF6 as shown in Fig.4.9 and results reveal that the level of ATF6 significantly ($p<0.01$) reduces in the DC group as compared to the NC group. Moreover, after treated with REP a significant ($p<0.001$) increment in the level of the ATF6 expression was observed with respect to DC which suggests that REP enhances the level of ATF6 and might help to reduce the apoptosis process. As ATF6 is activating transcription factor that activates the genes for the unfolded protein response during endoplasmic reticulum stress.

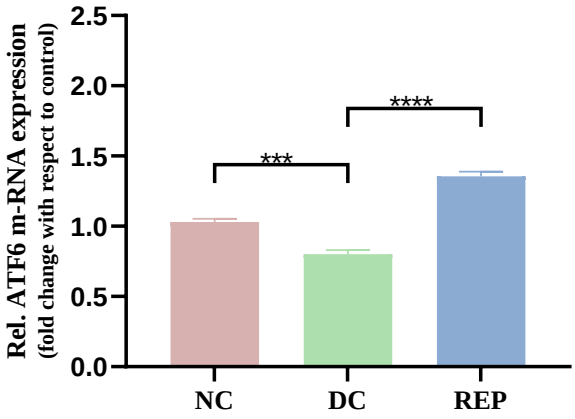

Fig.4.9: Effect of REP on the ATF6 expression. values are represented in mean ± SEM and *** Indicates *P< 0.001,* **** *P< 0.0001* by one-way ANOVA followed by Tukey's post hoc multiple comparison test

4.2.3.2 Western blot analysis

The Bax, and Bcl-2 both are apoptotic and anti-apoptotic protein respectively, whereas caspase-3 is the major effector of apoptosis, and activation of it cause irreversible cell death. Moreover, these proteins' (Bax, Bcl-2, and caspase-3) expression exerts a significant effect on neuron injury. In this study, the effect of REP on the expression of these proteins was measured and it was observed that the expression level of Bax and caspase increased significantly in the DC group compared to the NC group as shown in Fig.4.10. Moreover, the expression of Bcl-2 is reduced and indicates the occurrence of apoptosis in the DC group rats. After treatment with REP, the level of Bax reduces by 1.56-folds and caspase-3 by 1.04-folds compared to the DC group. It was also observed that the expression of Bcl-2 was increased by 1.4-fold compared to the DC group. Further, the overall results revealed that after administration of REP the expression of Bax, and caspase-3 reduced, whereas the expression level of Bcl-2 improved which represents that REP helps to reduce neuron cell death and has the potential to act as a neuroprotective agent.

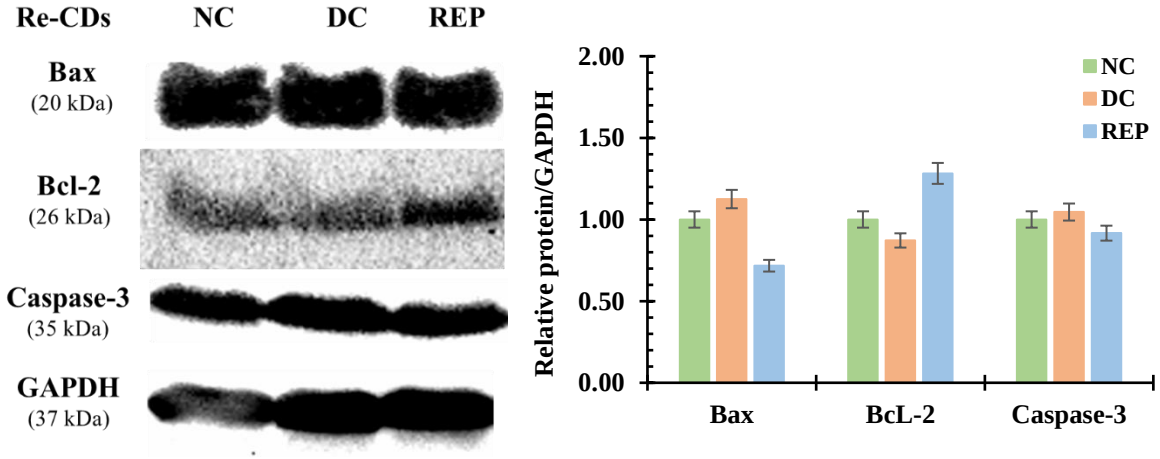

(A) **(B)**

Fig.4.10: Western blot analysis exhibited (A) Bcl-2, Bax, Caspase-3 and GAPDH expression in lysate from rats brain; (B) quantitative analysis of protein expression

In summary, REP was used to measure its neuroprotective effect by performing *in vitro* and *in vivo* assays as these methods were more reliable and prominent to estimate the effect. *The in vitro* assays suggested that as the concentration of REP increased, the cell viability of cells was reduced suggesting a dose-dependent response. Moreover, the designed *in vitro* studies also indicate the improvement in cell viability after being treated with REP in the STZ and peroxide-induced SHSY-5Y cells. The STZ generates stress in cells and induces phosphorylation of tau protein whereas peroxide produces oxidative stress in the cells.

Furthermore *in vivo* studies revealed that after treatment with REP (4 mg/kg,*p.o*) for 4 weeks in HFD-fed STZ wistar rats, a significant ($p<0.01$) decrement in Aβ, tau proteins, TNF-α, IL-6, MDA, NO, and increment in BDNF, SOD, GSH level was observed compared to disease control rats. Likewise, the behavioral studies i.e., PAT and MWZ showed a significant improvement ($p<0.01$) in the retention memory and spatial memory after the REP treatment compared to HFD-fed STZ group rats. Additionally, the apoptosis marker proteins (Bcl-2, Bax, Caspaase-3) and ATF6 gene expression in brain homogenate showed a significant ($p<0.05$) increase in Bcl-2, ATF-6 expression, and decrement in Bax, Caspase-3 expression after treated with REP indicates a reduction in neuronal cell death then the disease rats.

Based on the *In vitro* and *In Vivo* results, we further planned to circumvent the observed problems *i.e;* low absorptivity, high protein binding, first-pass metabolism, and poor pharmacokinetic and pharmacodynamic of REP, the targeted nano drug delivery systems were developed, and biologically evaluated.

4.3. Development and biological evaluation of Polymeric nanoparticles (PNPs)

4.3.1 Synthesis and characterization of di-block amphiphilic polymer

The mPEG-PCL polymer was synthesized using tin (II) 2-ethyl hexanoate as a catalyst with a simple ring-opening polymerization reaction of ε-caprolactone. The characterization of the amphiphilic di-block mPEG-PCL polymer was done by GPC and ^{1}H-NMR (Fig.4.11). The ^{1}H-NMR data confirmed the synthesis of mPEG-PCL di-block co-polymer as the spectrum shows peaks at δ 1.39, 1.66, 2.32, and 4.07, which signifies polycaprolactone formation whereas, characteristic peaks at δ 3.66 and 3.39 shows the presence of methylene units of PEG.

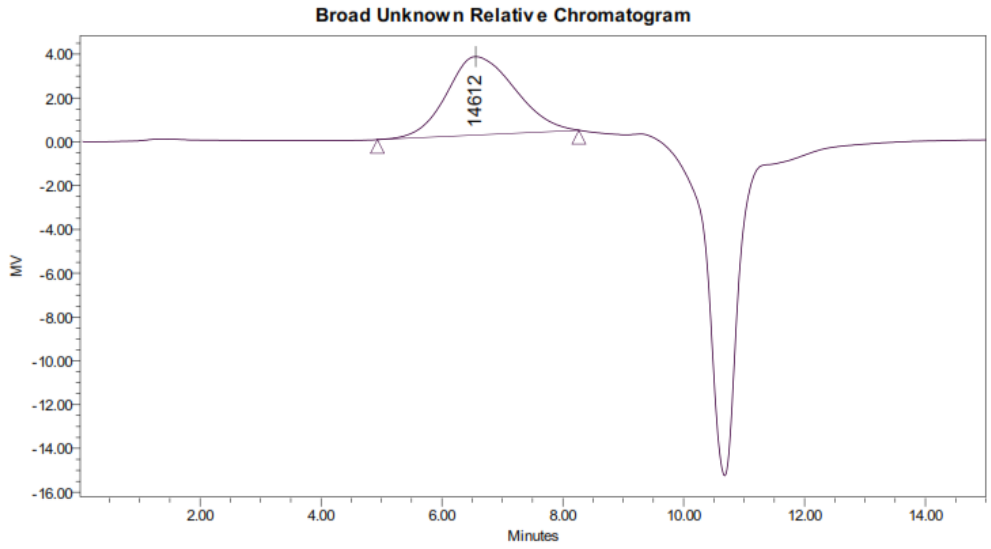

Broad Unknown Relative Peak Table

	Distribution Name	Mn (Daltons)	Mw (Daltons)	MP (Daltons)	Mz (Daltons)	Mz+1 (Daltons)	Polydispersity	Mz/Mw	Mz+1/Mw
1		11715	18298	14612	41318	124418	1.561870	2.258086	6.799557

(A)

Fig.4.11: Confirmation of the amphiphilic di-block polymer (PEG-PCL) was done by GPC[52]

4.3.2 Fabrication of PNPs

The PNPs were fabricated with synthesized di-block amphiphilic polymer using mPEG as a hydrophilic moiety and a hydrophobic PCL, which have higher biocompatibility and biodegradability. Here, mPEG behaves as a capping agent and acts as a shield for the growing nanoparticles, therefore the particle cannot expand after a certain extent. However, PCL a semicrystalline polymer is used for long-term drug delivery applications due to its slow diffusion and non-toxic nature. Herein, the polymerization of PEG-PCL is used to reduce immunogenicity, toxicity, prolong the blood circulation time and optimize protein activities.

4.3.3 Optimization of PNPs by QbD approach

The optimization of PNPs was done by the QbD approach using the design of experiments, and response surface methodology BBD. The response surface methodology was investigated for determining the difference between variables. Initially, the QTPPs were selected to ensure the safety and efficacy of the final product. The CQAs which are product quality attributes were selected from the QTPPs and influenced the finished product. Though the CQAs were evaluated and based on the parameters of the sequential model sum of the square, model summary statistic the model was suggested (Table 4.1), and quadratic model was recommended for PS (Response 1), PDI (Response 2) and EE (Response 3).

Table 4.1: The Statistical values for each of the model sources for both the responses, along with remarks generated by the Design-Expert® software (version 13.0, Stat-Ease Inc.) under the heading of summary of fitness of each model.

	Response	Source	Sequential p value	R^2	Adjusted R^2	Predicted R^2	Press	Remarks
PNPs	Particle size	Liner	0.0026	0.6524	0.5722	0.3621	22264.95	-
		2FI	0.9089	0.6700	0.4721	-0.3226	46162.34	-
		Quadratic	**<0.0001**	**0.9852**	**0.9661**	**0.9227**	**2696.65**	**Suggested**
		Cubic	0.7306	0.9889	0.9557	-	-	Aliased
	PDI	Liner	0.0114	0.5605	0.4591	0.2061	0.1159	-
		2FI	0.7276	0.6120	0.3792	-0.4692	0.2145	-
		Quadratic	**<0.0001**	**0.9902**	**0.9776**	**0.9377**	**0.0091**	**Suggested**
		Cubic	0.6162	0.9935	0.9739	-	-	Aliased
	Entrapment efficiency	Liner	0.0011	0.6958	0.6256	0.5124	2661.61	-
		2FI	0.9279	0.7088	0.5341	0.1240	4781.29	-
		Quadratic	**< 0.0001**	**0.9901**	**0.9773**	**0.9424**	**314.23**	**Suggested**
		Cubic	0.6732	0.9930	0.9719	-	-	Aliased

Furthermore, the ANOVA was applied to evaluate the factors which affect the response in quadratic equations (Table 4.2). It was observed that the drug-polymer ratio (Factor 1), surfactant concentration (Factor 2), and sonication time (Factor 3) significantly affect selected responses in PNPs. The BBD provides information on polynomial equations involved in the interaction, the effects of independent variables, and their responses.

Table 4.2: Statistical validation parameters of the selected models for individual responses of PNPs

Response	Equation	Adequate precision	F-value	*p*-value Prob >F
Particle size	$+122.27+50.08A+5.91B-17.42C-11.59AB+3.57AC-2.58BC+49.31A^2-8.34B^2+9.82C^2$	22.60	51.67	0.0001
PDI	$+0.11+0.09A-0.006B-0.02C-0.01AB$ $0.03AC+0.01BC+0.11A^2+0.02B^2-0.007C^2$	25.90	78.73	0.0001
Entrapment	$+73.74+8.30A-14.03B-14.45C$ $+3.44AB-2.21AC-1.02BC-6.36A^2-3.68B^2-16.94C^2$	27.62	77.84	0.0001

Attentively observing the polynomial equations and surface plots (2d or 3d) results in emphasizing the effects of each variable independently and in combination with other variables on each response. The 3D response surface plots of PS, PDI, and % EE on PNPs were generated and showed a dependency on selected independent variables (Fig.5.22). It was examined that as the drug: polymer ratio increases, the PS, PDI, and % EE increase. Herein, the amount of the drug was kept constant, and changes in the amount of polymer were carried out. As the amount of polymer increased, it resulted in a decrease in PS and PDI due to the change in concentration of hydrophilic moiety of the polymer. Moreover, a reduction in PS, PDI, and % EE is observed as the surfactant concentration and sonication time increase. The increase in

surfactant concentration leads to adsorption onto the interface and reduces the surface tension, whereas an increase in the sonication time breaks the particles and reduces the dispersion size.

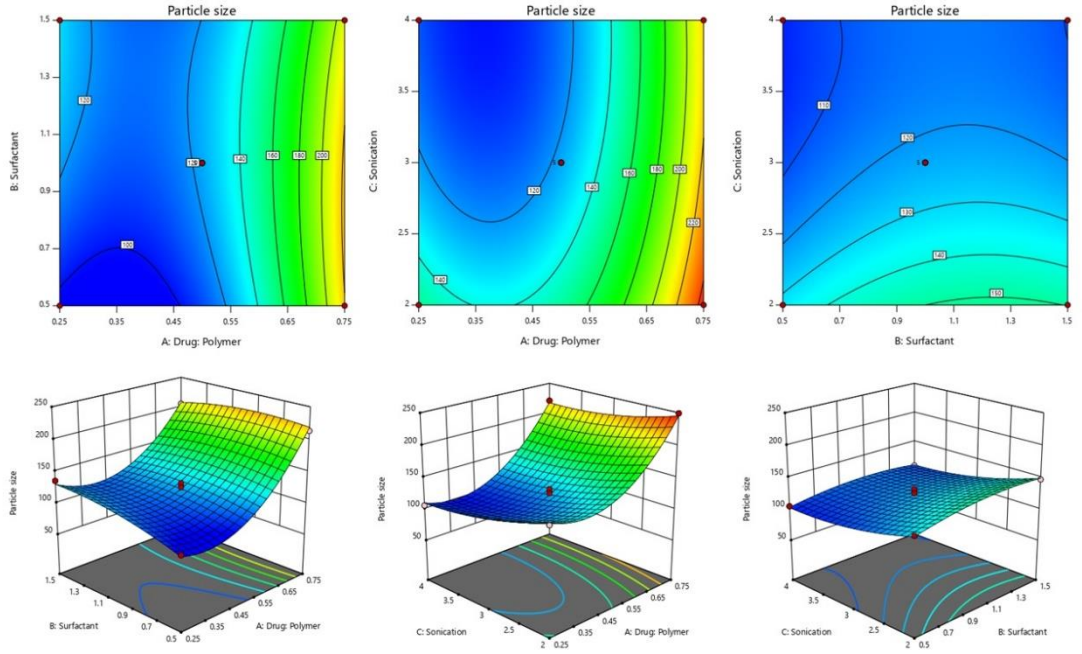

(A)

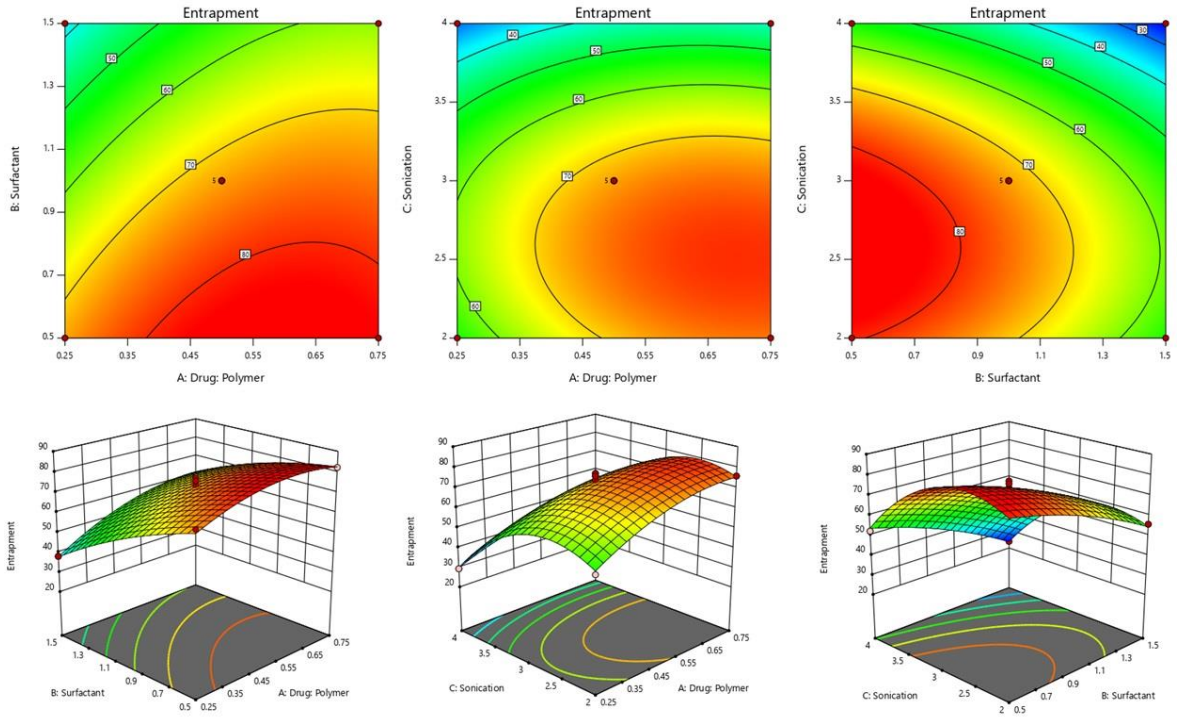

(B)

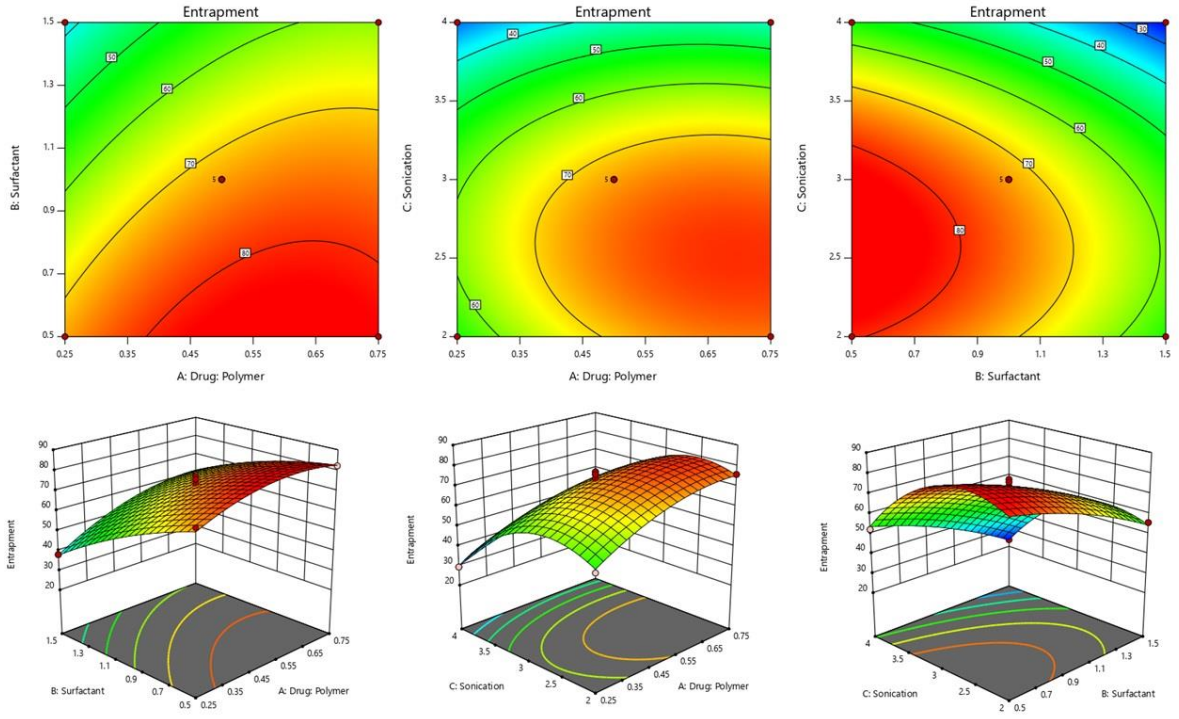

(C)

Fig.4.12: The 2D and 3D-response surface plot showing the relationship among the factors on (A) particle size, (B) PDI, and (C) entrapment efficiency of Drug: polymer; Surfactant amount (AB factor), Drug: polymer; Sonication time (AC factor), Surfactant, sonication time (BC factor) of the PNPs

The overlay plot was created by numerical and graphical methods to predict the composition for optimizing the nanoformulation. The composition of factors was selected from the design space in the overlay plot (Fig.4.13) and the selected criterion for the optimized region was to obtain by minimum PS, PDI, and maximum EE%.

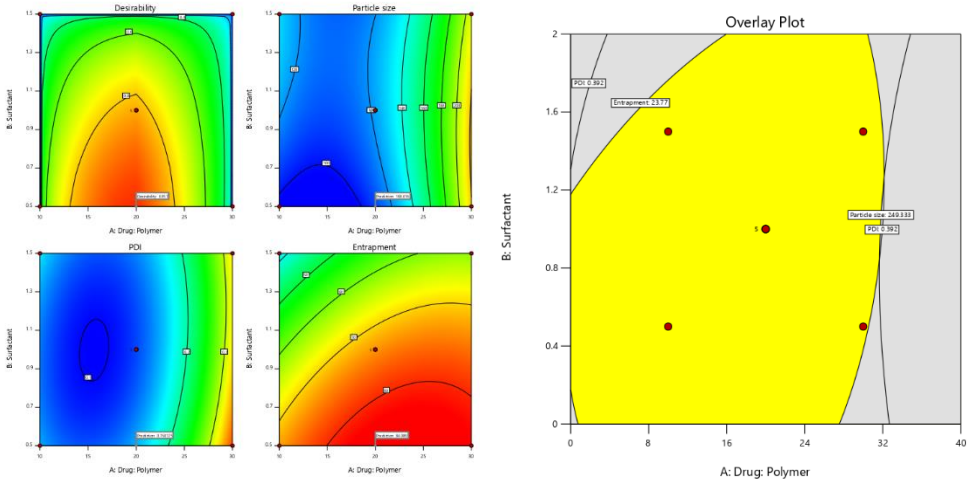

(A) **(B)**

Fig.4.13: The (A) desirability index and (B) overlay plot of PNPs with Drug: polymer; Surfactant amount (AB factor)

Furthermore, the predicted results were validated by comparing them with the actual experimental values obtained from the responses (Table.4.3). The deviation between predicted and experimental values ranged from -4.33 to 5.42 in PNPs. The obtained results demonstrated that the generated design space can reduce the risk of failure and thus indicated that the models are reliable.

Table 4.3: Experimental design model validation

Responses		Polymeric nanoparticles		
		Predicted value	**Experimental value**	**% Residual**
Particle size	(nm)	108.01	112.53 ± 5.91	-4.33
Polydispersity index	-	0.166	0.157 ± 0.08	5.42
Entrapment efficiency	(%)	84.08	77.78 ± 3.98	4.04

4.2.4 Development and biological evaluation of Polymer lipid hybrid nanoparticles (PLHNPs)

4.2.4.1 Preparation of polymeric lipid hybrid nanoparticles (PLHNPs)

The PLHNPs were formulated by different phospholipids in combination with four different stabilizers. The amount of lipids used was 20% w/w of the amount of PLGA and the stabilizer concentration was 0.5% w/v for all the trial experiments. Firstly, the stabilizers including Tween 80, PVA, Pluronic F127, and TPGS were screened, and characteristic parameters were evaluated. Based on the PS, PDI, and EE, it was observed that Pluronic F127 showed comparatively the smallest PS with the highest EE and was graded the best among all. Pluronic F127 is the grade of poloxamer which is a triblock copolymer of ethylene oxide (EO) and propylene oxide (PO), that aids to form a self-assembled hydrophilic outer shell of polymer lipid surface. Through reports, it was ascertained that Pluronic F127 enhances EE and reduces PS. Although the phospholipids were screened (Phospholipon-90 H, Soy lecithin, Egg Phosphatidylcholine, Soy Phosphatidylcholine) to assess the effect of different phospholipids. It was observed that PLHNPs with SPC show good characteristic properties among all such as smaller PS, less PDI, and high EE (Table.4.4). Further, PLGA, SPC, DSPE-PEG_{2000}, and Pluronic F127, were used in the preparation of PLHNPs, due to their biodegradable, biocompatible properties, and approved by the Food and Drug Administration (FDA) as drug carriers for clinical use. The PLGA is a hydrophobic polymer that precipitates to form a hydrophobic core for the encapsulation of drug and SPC a phospholipid, which forms the lipid monolayer at the interface of the PLGA core. The PEGylated lipid (DSPE-PEG_{2000}) helps to

form the "stealth" shell of the PLHNPs. However, SPC and DSPE-PEG_{2000} conjugate and self-assemble around the hydrophobic core to form a lipid monolayer.

Table.4.4: Preliminary Screening of phospholipids & stabilizers for preparation PLHNPs. Data are represented as mean ± SEM (n=3)

Formulation No.	Phospholipids	Stabilizers	Particle size (nm)	Polydispersity index	Entrapment efficiency (%)
F1	Phospholipon-90 H	Tween 80	166.55 ± 3.41	0.125 ± 0.07	10.72 ± 2.97
F2		PVA	188.00 ± 2.94	0.133 ± 0.08	32.22 ± 3.86
F3		Pluronic- 127	178.86 ± 1.76	0.186 ± 0.09	31.23 ± 5.96
F4		TPGS	251.15 ± 2.87	0.212 ± 0.10	6.53 ± 3.37
F5	Soy lecithin	Tween 80	178.10 ± 4.12	0.140 ± 0.06	25.37 ± 3.18
F6		PVA	174.10 ± 3.49	0.146 ± 0.14	56.68 ± 4.61
F7		Pluronic- 127	186.76 ± 3.56	0.249 ± 0.11	41.65 ± 2.71
F8		TPGS	191.33 ± 2.97	0.262 ± 0.15	23.71 ± 2.97
F9	Egg Phosphatidylcholine	Tween 80	185.53 ± 1.65	0.238 ± 0.21	45.94 ± 2.98
F10		PVA	163.03 ± 2.76	0.168 ± 0.23	41.24 ± 5.90
F11		Pluronic- 127	175.30 ± 3.94	0.160 ± 0.26	50.84 ± 3.97
F12		TPGS	173.86 ± 2.45	0.153 ± 0.09	24.69 ± 3.76
F13	Soy Phosphatidylcholine	Tween 80	183.60 ± 4.76	0.144 ± 0.16	37.50 ± 3.87
F14		PVA	178.53 ± 3.87	0.188 ± 0.17	50.53 ± 4.29
F15		Pluronic- 127	164.56 ± 2.95	0.158 ± 0.19	60.90 ± 4.76
F16		TPGS	170.13 ± 2.78	0.166 ± 0.11	9.59 ± 4.57

4.2.4.2 Optimization of PLHNPs by QbD approach

The optimization of PLHNPs by the QbD approach was done by selecting QTPPs and CQAs to ensure the safety and efficacy of the product. However, CQAs were evaluated, and based on the parameters of the sequential model sum of the square, model summary statistic the model was suggested (Table.4.5).

Table.4.5.: The Statistical values for each of the model sources for both the responses, along with remarks generated by the Design-Expert® software (version 13.0, Stat-Ease Inc.) under the heading of summary of fitness of each model.

Response	Source	Sequential p value	R^2	Adjusted R^2	Predicted R^2	Press	Remarks
Particle size	Liner	**<0.0001**	**0.8598**	**0.8279**	**0.7489**	**1807.24**	**Suggested**
	2FI	0.7592	0.8747	0.7995	0.5322	3367.04	-
	Quadratic	0.5368	0.9064	0.7860	0.0574	6784.36	-
	Cubic	0.2691	0.9615	0.8461	-	-	Aliased
PDI	Liner	0.1068	0.3643	0.2176	0.1748	0.0869	-
	2FI	0.7402	0.4360	0.0976	-0.3036	0.1373	-

	Quadratic	**0.0025**	**0.9188**	**0.8406**	**0.0726**	**0.0977**	**Suggested**
	Cubic	0.2111	0.9708	0.9479	-	-	Aliased
	Liner	0.6488	0.1150	-0.0892	-0.4667	11330.01	-
Entrapment	2FI	0.5835	0.2652	-0.1757	-1.1717	16775.86	-
efficiency	Quadratic	**< 0.0001**	**0.9746**	**0.9420**	**0.8133**	**1442.03**	**Suggested**
	Cubic	0.5170	0.9848	0.9393	-	-	Aliased

The linear model was suggested for Response 1(PS) whereas the quadratic model was recommended for Response 2 (PDI) and Response 3(EE) based on the applied ANOVA test to evaluate the factors which affect the response in quadratic equations (Table.4.6).

Table.4.6: Statistical validation parameters of the selected models for individual responses

	Response	**Equation**	**Adequate precision**	**F-value**	***p*-value Prob >F**
PLHNPs	Particle size	+133.20-0.17A-0.35B-27.81C	13.18	26.58	0.0001
	PDI	+0.18+0.05A+0.01B-0.05C+0.008AB+ 0.002AC+0.033BC+0.02A^2+0.34B^2+0.01C^2	8.69	13.88	0.0045
	Entrapment	+64.21+18.56A+5.82B+6.36C+1.64AB-7.36AC+7.90BC-7.44A^2-17.51B^2-4.56C^2	14.49	65.28	0.0001

It was observed that the selected factors i.e., drug-polymer ratio (Factor 1), amount of lipid (Factor 2), and sonication time (Factor 3) significantly affect PS, PDI, and EE in PLHNPs. The BBD provides information on polynomial equations involving the interaction, effects, and responses of independent variables. Attentively observing the polynomial equations and surface plots (2d or 3d) results in emphasizing the effects of each variable independently and in combination with other variables on each response.

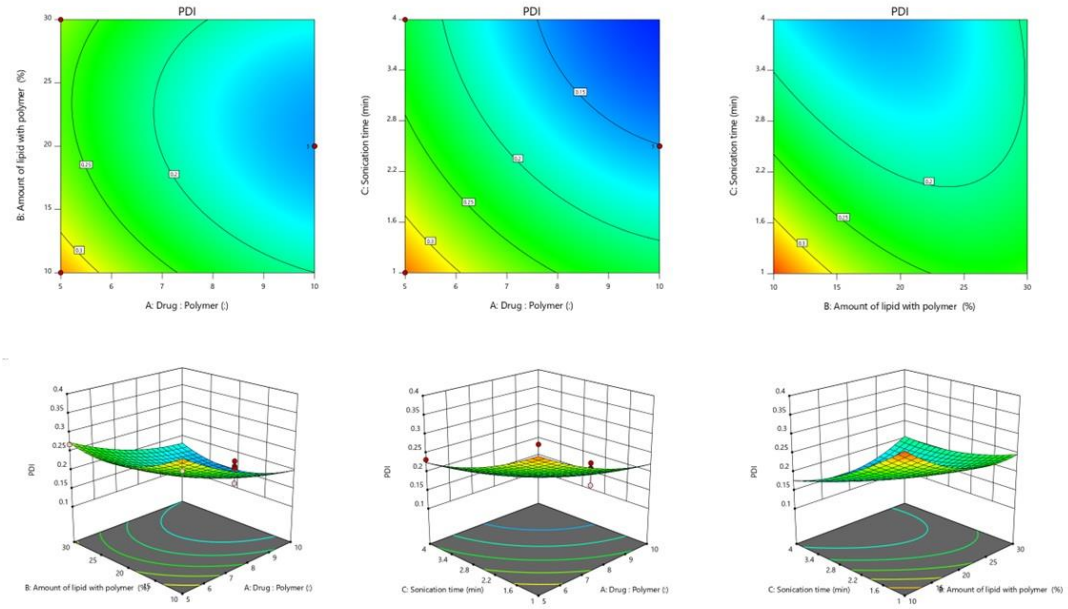

(A)

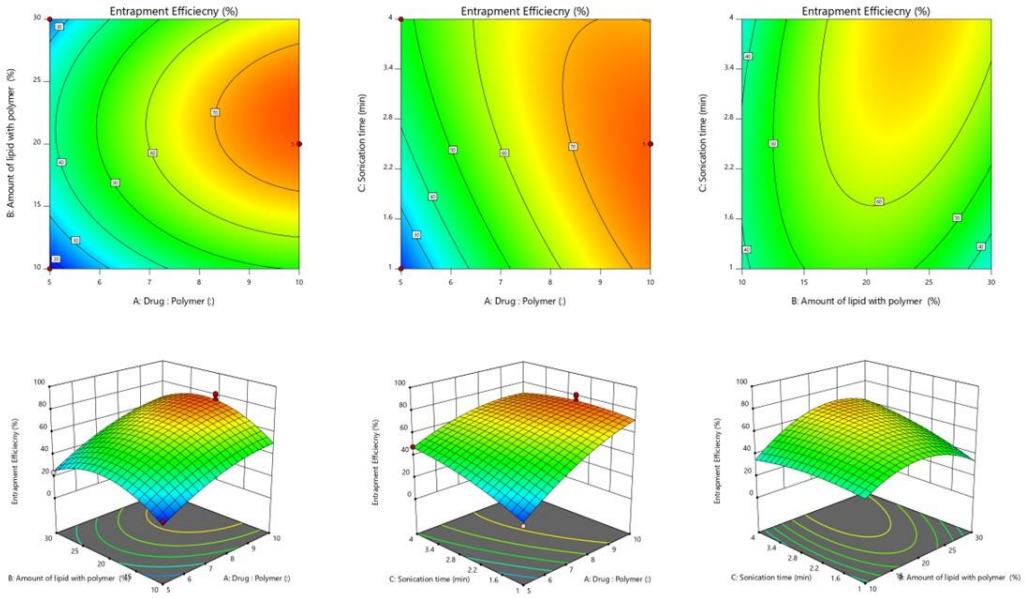

(B)

Fig. 4.14: The 2D and 3D-response surface plot showing the relationship among the factors on (A)PDI, and (B) entrapment efficiency of Drug: polymer; Surfactant amount (AB factor), Drug: polymer; Sonication time (AC factor), Surfactant, sonication time (BC factor) of the PLHNPs

The 2D and 3D response surface plots of PS, PDI, and % EE on PLHNPs were generated (Fig.4.14 A-B) and showed a dependency on selected independent variables. It was observed that the PS, PDI, and % EE increase as the drug: polymer ratio increases. However, the drug amount was kept constant while the amount of polymer was varied (increased) resulting in a decrease PS and PDI due to the change in concentration of hydrophilic moiety of the polymer. Moreover, an increase in the amount of lipid enhances the EE due to an increase in the viscosity of the medium resulting in rapid solidification which prevents drug diffusion and leads to a greater or speedy encapsulation. In addition, sonication time increased, PS, PDI, and percent EE were observed to decrease. An increase in sonication time breaks up the particles and decreases the dispersion size. The overlay plot was obtained using numerical and graphical methods to predict the optimal composition for PLHNPs [53]. The composition of factors was selected from the design space in the overlay plot (Fig.4.15) and the minimum PS, PDI, and maximum EE% were kept for the selected criterion for the optimized region.

In addition, the predicted results were verified by comparing them with the actual experimental values derived from the responses (Table.4.7). In PLHNPs, the deviation between predicted and experimental values varied from -1.86 to 4.91. The obtained results demonstrated that the generated design space can reduce the risk of failure and thus indicated that the models are reliable.

Table.4.7: Experimental design model validation of PLHNPs by QbD.

Responses		Polymeric lipid hybrid nanoparticles		
		Predicted value	**Experimental value**	**% Residual**
Particle size	(nm)	130.01	125.09 ± 3.21	4.91
Polydispersity index	-	0.16	0.18 ± 0.05	-0.02
Entrapment efficiency	(%)	73.37	75.23 ± 1.94	-1.86

4.4. Physicochemical Characterization of nanoparticles

4.4.1 Particle size and morphological evaluation

PS is a crucial parameter that influences the release, stability, *in vitro* and *in-vivo* pattern. The absolute size of PNPs and PLHNPs was found to be 112.53 ± 5.91nm and 125.09 ± 3.21 nm respectively. Whereas the PDI of PNPs was observed at 0.157 ± 0.08 and for PLHNPs was 0.18 ± 0.05. Additionally, the ZP of PNPs and PLHNPs was found to be -6.20 ± 0.82 mV and -16.4 ± 0.53 mV (Fig.4.16 A-B). In PS, PDI, and ZP no significant changes were observed between PNPs and PLHNPs. All the characteristics parameters were in the nano range with PS <150 nm, PDI <0.3, and ZP in between ±30 mV[54].

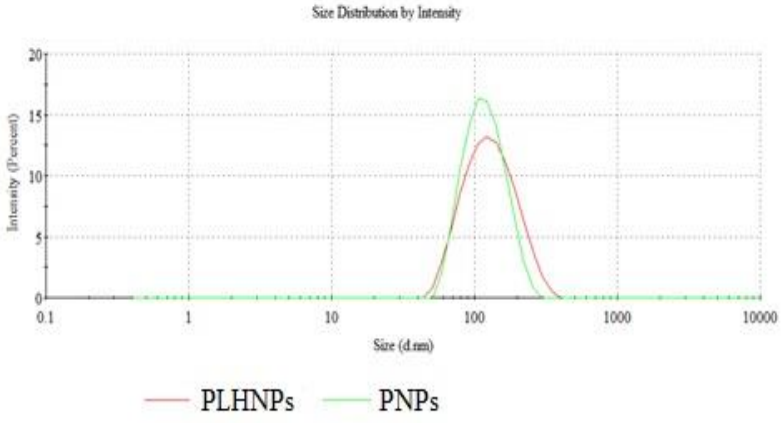

(A)

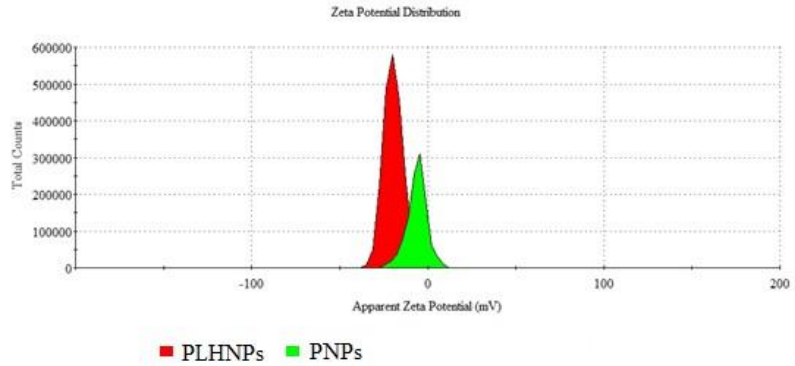

(B)

Fig.4.16: Characterization of Polymeric nanoparticles and polymer lipid hybrid nanoparticles by (a) particle size, (b) zeta potential

Moreover, particle morphology significantly influences the percent drug loading, entrapment efficiency, drug release profile, pharmacokinetics, and biodistribution pattern of the nanoparticles. It also has a role in cellular uptake, cellular internalization, receptor binding, and molecular interactions. The FE-SEM and TEM analysis showed that most nanoparticles were isometric, with smooth surfaces and the average size of nanoparticles was the same as obtained by DLS. However, in TEM the PLHNPs showed a spherical core-shell structure in which the core (PLGA) was properly surrounded by lipid monolayer at the interface (Fig.4.17. A&B).

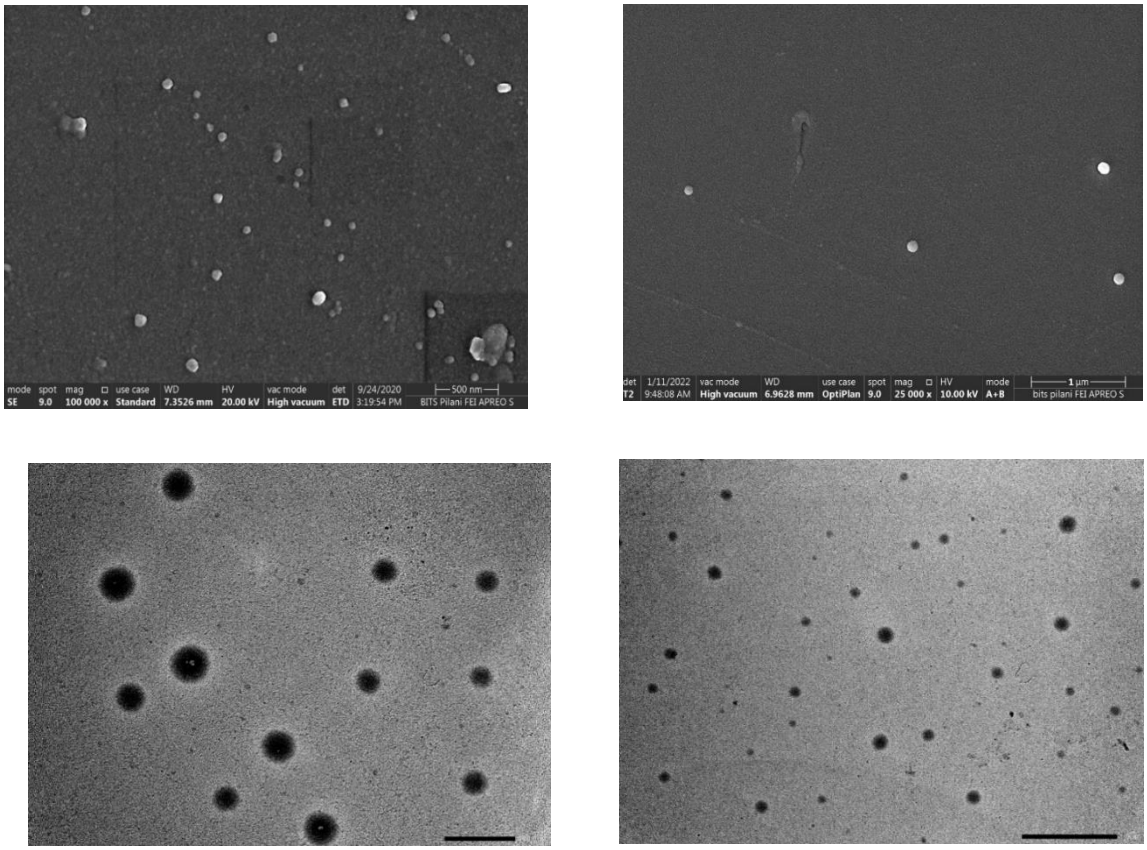

(A) **(B)**

Fig.4.17: Morphological characterization of polymer lipid hybrid nanoparticles by (A) PNPs and (B) PLHNPs

4.4.2 *In vitro* drug release study

The estimation of the release profile of REP, PNPs and PLHNPs is important to understand the rate and extent of the drug present at the site of action. The controlled release of drugs is essential to maintain the therapeutic window. Hence a sustained/controlled release of drug from nanoparticle is suitable to maintain the therapeutic window. The release profile of, PNPs and

PLHNPs were estimated (Fig.4.18) and showed a cumulative drug release of ~ 70% and ~58% respectively within 48h respectively. The observed release profile data shows that PLHNPs have more sustainability than PNPs due to the core-shell structure of PLHNPs which decreases the diffusion rate and is sustained for a longer period.

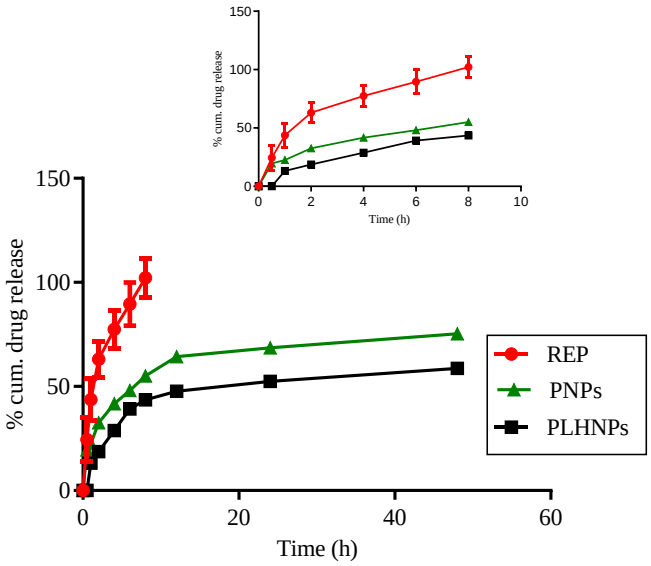

Fig.4.18*: In vitro* release profile of REP and PLHNPs using dialysis bag method for 48h.

Although, various mathematical models were measured to determine the release pattern of REP using DD-Solver (Table.4.8). It was observed that the REP follows the first order kinetics whereas PNPs and PLHNPs featured with low AIC value with high regression coefficient and fitted to the Korsmeyer-Peppas model which indicates that NPs imply the degradation by creating fine pores with diffusion.

Table.4.8: Mathematical models of release profile

Model	**Parameters**	**Test Sample**		
		REP	**PNPs**	**PLHNPs**
Zero	K_0	9.03	4.31	3.48
	R^2	0.69	0.83	0.80
	AIC	108.37	81.66	74.63
First	K_1	2.16	0.13	0.07
	R^2	0.94	0.97	0.91
	AIC	84.90	72.52	67.05
Higuchi	K_H	39.52	19.09	14.92
	R^2	0.85	0.94	0.92
	AIC	96.41	68.33	58.58
Korsmeyer-Peppas	$_K$KP	81.82	34.55	20.62
	R^2	0.93	0.98	0.95
	AIC	73.76	42.79	55.01

4.4.3 Stability study in simulated biological fluids

Nano formulations for the controlled delivery of drugs are receiving considerable attention, but the stability of nanoparticles has been a source of concern. Particularly, the size and dispersity of nanoparticles that facilitates target-specific delivery, rapid gastric emptying, and reproducible GIT transit. In addition, it safeguards the encapsulated drug, controlled release profile, decreased toxicity, and immunogenic potential more effectively than the conventional system. In the preparation of nanoparticles, surface-capping or stabilizing ligands were used to regulate particle dimensions. As depicted in Fig.4.19, the PLHNPs were found to be stable in simulated gastrointestinal fluids, and a significant change in their quality attributes was observed. As the formulation contains a stabilizing or capping agent (Poloxamer), van der Waals forces are diminished, and repulsive forces are established between the colloidal particles. These forces ultimately diminished particle aggregation and precipitation. The PLHNPs were comprised of biodegradable polymers and DSPE-PEG2k a PEG-Lipid which aims to improve the stability and mobility of the complexes in the harsh gastrointestinal environment compared to PNPs.

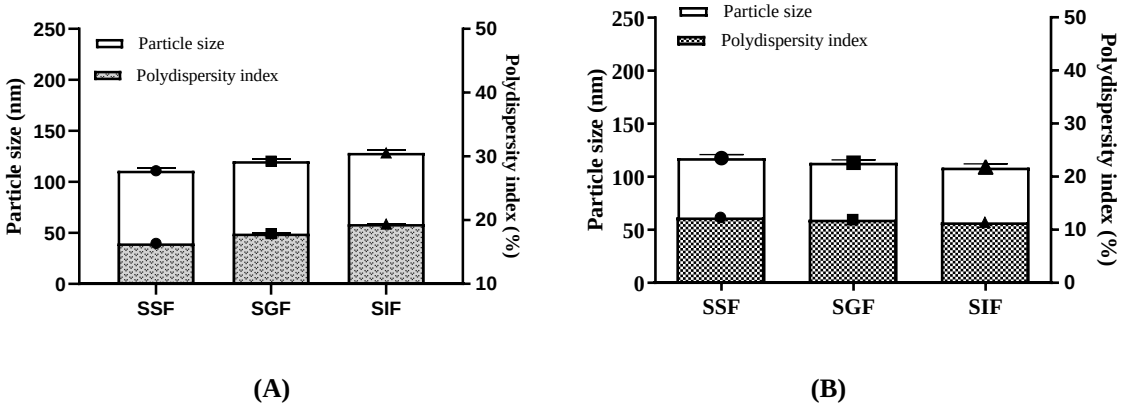

Fig:4.19: Stability study of (A) PNPs and (B) PLHNPs in simulated gastrointestinal fluids

4.4.5 Permeability assessment

4.4.5.1 *In situ* absorption study by Single pass intestinal perfusion (SPIP) model

Intestinal absorption is a crucial factor for defining the bioavailability of oral drugs, as there are many transporters that are available on the intestine which are involved in the pharmacokinetic profile of drugs.[43,46] Thus, intestinal absorption plays a critical role in their improvement, safety, and effectiveness.[55] In the study, it was observed that the P_{eff} value increased around ~ 2.3 folds of PNPs and ~ 3.3 folds PLHNPs compared to free REP and showed a significant change in intestinal permeation rate (Fig.4.20). Additionally, the K_a is also increased by ~2.3folds in PNPs and ~3.9 fold in PLHNPs with respect to REP indicating that the nano formulations enhanced the permeation/absorption rate of REP in wistar rats.

Though the PLHNPs show more significant enhancement (~3.13-fold P_{eff} & ~1.69-fold K_a) in comparison to PNPs, it may be due to more GIT stability or can be attributed to the core-shell structure of PLHNPs which helps to maintain the controlled release of the drug and also enhance permeation [56].

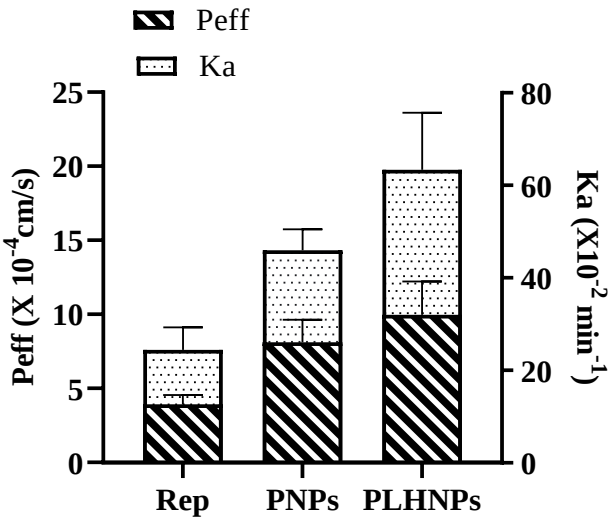

Fig.4.20: Effective permeability coefficient and apparent absorption rate constant of PNPs and PLHNPs after using SPIP wistar rat model

4.4.5.2 Parallel artificial membrane permeability assay-blood brain barrier

The PAMPA-BBB is the most used method to predict brain permeability due to its high throughput and is designed to precisely mimic the physicochemical microenvironment of the barrier. PAMPA is a limited method because it is modeled by an artificial membrane and thus is neither used for active transport nor P-gp efflux. Herein, REP and PLHNPs were examined to determine the effective permeability (Pe) using measured concentrations and it was observed that the PNPs achieved ~1.3 folds and PLHNPs ~1.6 folds more permeability to the brain than REP due to the core-shell structure of the nanoparticles which enhanced the selective tissue targeting and sustain the release profile [48,49,57].

4.4.6 *In vitro* cell culture study

4.4.6.1 Cell viability assay

in vitro cell culture studies were performed on neuroblastoma SHSY-5Y cells to measure the effect of both the formulations (PNPs and PLHNPs) on cell viability, cellular uptake, etc. It was revealed that more than 70% of cells were viable in the blank formulation which indicates that both the formulations were biocompatibility and nontoxicity (Fig.4.21). Moreover, the

PLHNPs show ~90-95% cell viability whereas PNPs has cell viability of ~80-85% indicating the effectiveness of PLHNPs[58].

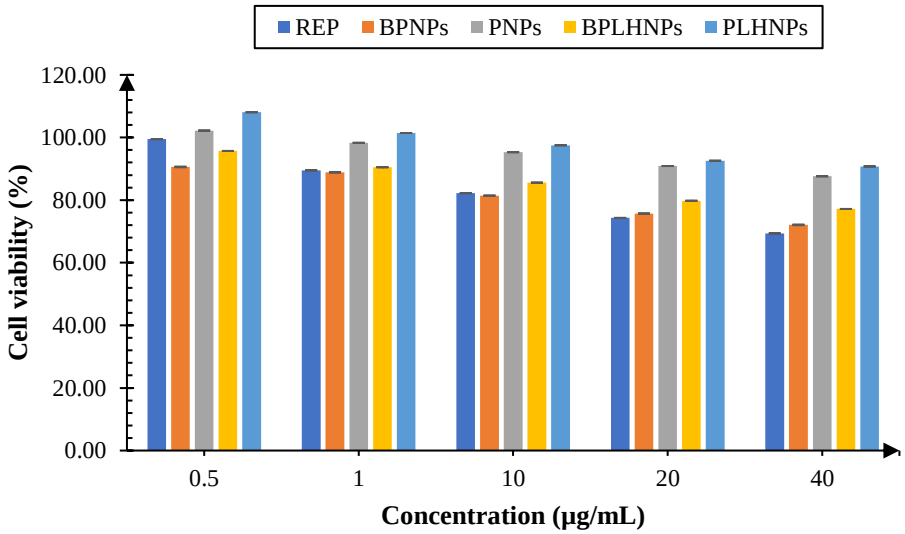

Fig.4.21: *In vitro* cell culture studies on neuroblastoma cell line SHSY-5Y for estimation of cell viability by MTT cytotoxicity assay.

4.4.6.2 Cellular uptake

The cellular uptake of both the formulations was quantified and observed that the PLHNPs showed ~ 1.2 % more uptake than the PNPs which could be due to the size-independent lipid trafficking pathway (Fig.4.22.) The lipid density in the cellular membrane increases the sustained drug release compared to PNPs. The PLHNPs easily affect the biological barriers and efficiently enhance circulation. Moreover, negative charge also exhibits a strong interaction with the cell membrane and therefore enhances the intercellular uptake. Though more uptake into the cells ensures more amount of the drug is available at the site of action for therapeutic activity indicating the possibility for reduction of dose and improvement in efficacy

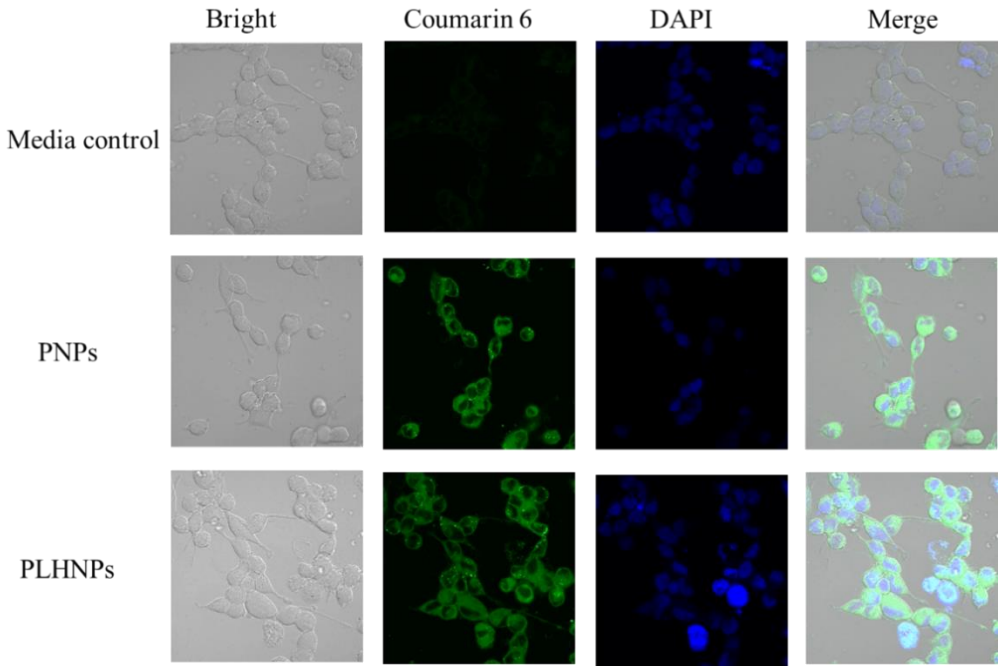

Fig.4.22: The quantitative estimation of coumarin 6, coumarin 6 loaded PNPs, and coumarin 6 loaded PLHNPs in cellular uptake study by (A) confocal microspore,

4.4.6.3 STZ treated SHSY-5Y cell-based study

The effect of REP, PNPs and PLHNPs on metabolic stress induced in cells was measured by performing an STZ cell study (Fig.4.23). Though it was observed that the PLHNPs represent an increment of ~1.67 fold and PNPs showed nearly ~1.2-fold increase in cell viability which represents a significant effect compared to only STZ-induced cells. However, REP enhances the viability of cells but after loading into PLHNPs the ~1.20-fold and PNPs ~1.1-fold improvement was also observed compared to REP in the STZ-induced SHSY-5Y cells.

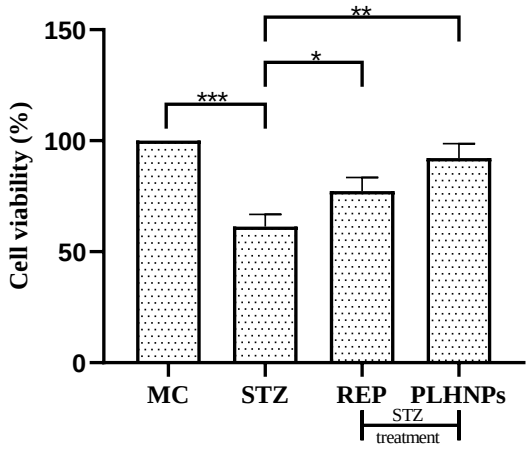

Fig.4.23: The effect of REP and PLHNPs on STZ-treated SHSY-5Y neuroblastoma cell lines Data are represented in (mean ± SEM, n=8 rats per group). * Indicates ** *P< 0.05;* ** *P< 0.01,* *** *P< 0.001,* by one-way ANOVA followed by Tukey's post hoc multiple comparison test

4.4.6.4 Reactive oxygen species-scavenging activity by hydrogen peroxide

The scavenging assay was performed to estimate the effect of REP, PNPs and PLHNPs on SHSY-5Y cells after being treated with 1 mM H_2O_2 for 12 h. Further, the study indicates that the REP shows a ~1.3-fold increase in cell viability, while PNPs, and PLHNPs show a significant ($p<0.01$) effect and enhance the effect by~1.3-fold and ~1.5-fold compared to H_2O_2 (Fig.4.24). The increase in cell viability indicates that the REP predominates the activity, whereas PLHNPs simultaneously enhance the protective effect.

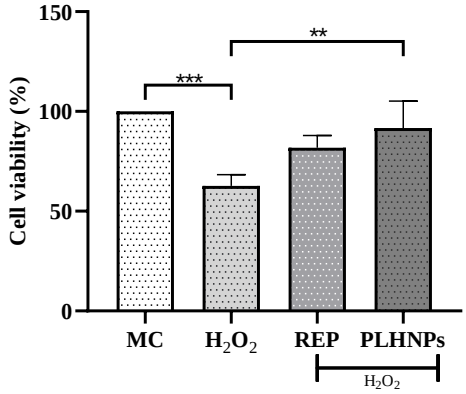

Fig.4.24: Neuroprotective effect of REP and PLHNPs on H_2O_2 treated SH-SY5Y neuroblastoma cell lines. Data are represented in (mean ± SEM, n=8 rats per group). * Indicates ** *P< 0.01,* *** *P< 0.001,* by one-way ANOVA followed by Tukey's post hoc multiple comparison test

4.4.7 Pharmacokinetic study

The pharmacokinetic studies for REP, PNPs and PLHNPs were investigated on wistar rats and the plasma concentration versus time profiles were plotted in Fig.4.25. The oral administration of PLHNPs results in good absorption, and peak plasma concentration reached in ~3.6 h approximately (Table.4.9). It was observed that the PLHNPs exhibited ~ 6.4-fold increase in t1/2 than REP solution, indicating slow distribution and elimination. However, AUC was observed to be higher in PLHNPs (32625.07 ± 3167.49 ng. h/ml) than in pure REP solution, which indicates the long-circulating ability of the nanoformulation in plasma. The clearance (Cl) of PNPs indicates ~1.8 fold, a decrease to pure REP solution. The increment in the PK parameters might be due to the core-shell of the lipid which influences the kinetic properties and DSPC-PEG_{2000} helps to increase the circulation time, protecting against immune recognition.

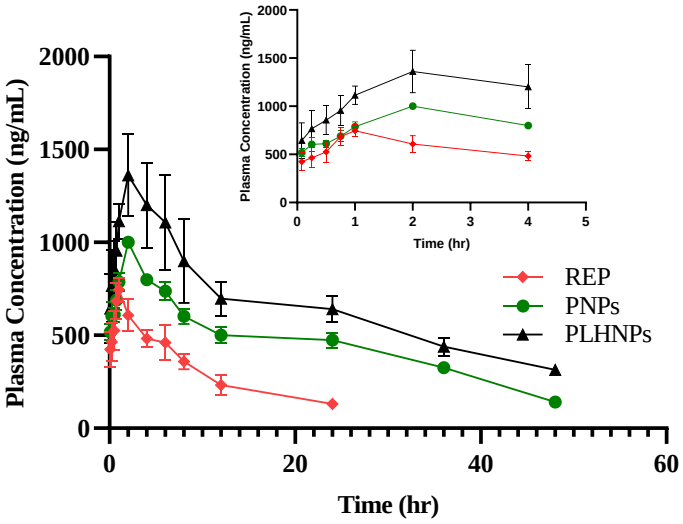

Fig.4.25: Plasma concentration-time profile of REP, and PLHNPs. Values were represented in mean ±SEM,

Table.4.9.: Pharmacokinetic parameters of REP, PNPs and PLHNPs

Parameters		REP	PNPs	PLHNPs
t_{max}	(h)	0.81 ± 0.19	2.00 ± 0.00	3.60 ± 1.16
C_{max}	(ng/mL)	800.76 ± 26.57	1001.09 ± 25.80	1547.16 ± 165.72
AUC	(ng.h/mL)	7441.69 ±763.75	21960.01 ± 907.09	32625.07 ± 3167.49
CL	(mL/h/kg)	163.84 ± 17.39	129.98 ± 27.152	88.87 ± 4.67
$t_{1/2}$	(h)	2.65 ± 1.54	15.91 ± 4.73	24.16 ± 2.19
MRT	(h)	8.24 ± 0.32	20.25 ± 0.21	38.633 ± 1.02

4.4.8 Biodistribution study

Biodistribution studies were performed to identify the potential nano-formulation for the brain targeting efficiency after oral administration. The REP distribution pattern was quantified in all the major organs (brain, heart, liver & kidney) and concentration-time profiles were represented in Fig.4.26. In the brain, the concentration levels of REP have observed for 12 h but for the PNPs and PLHNPs it continued for more than 24 h and exhibited ~3.5 fold ($p < 0.05$) increases in the brain uptake due to the presence of PEGylation on the outer surface of the nanoparticles. A similar pattern was observed in the heart where the REP shows the maximum concentration in 2h and observed for 12 h though PNPs, PLHNPs were still present for more than 24 h. As per the literature survey, REP was completely metabolized (98%) by oxidative biotransformation and direct conjugation with glucuronic acid. Interestingly, REP-loaded NPs showed a significant decrease in the metabolism of REP than the free REP which might be due to the presence of a core-shell structure that consists of biodegradable polymer

and target moieties attached over the surface. Moreover, REP has a very fast elimination rate and NPs lower the concentration of REP in the kidney and showed a sustained.

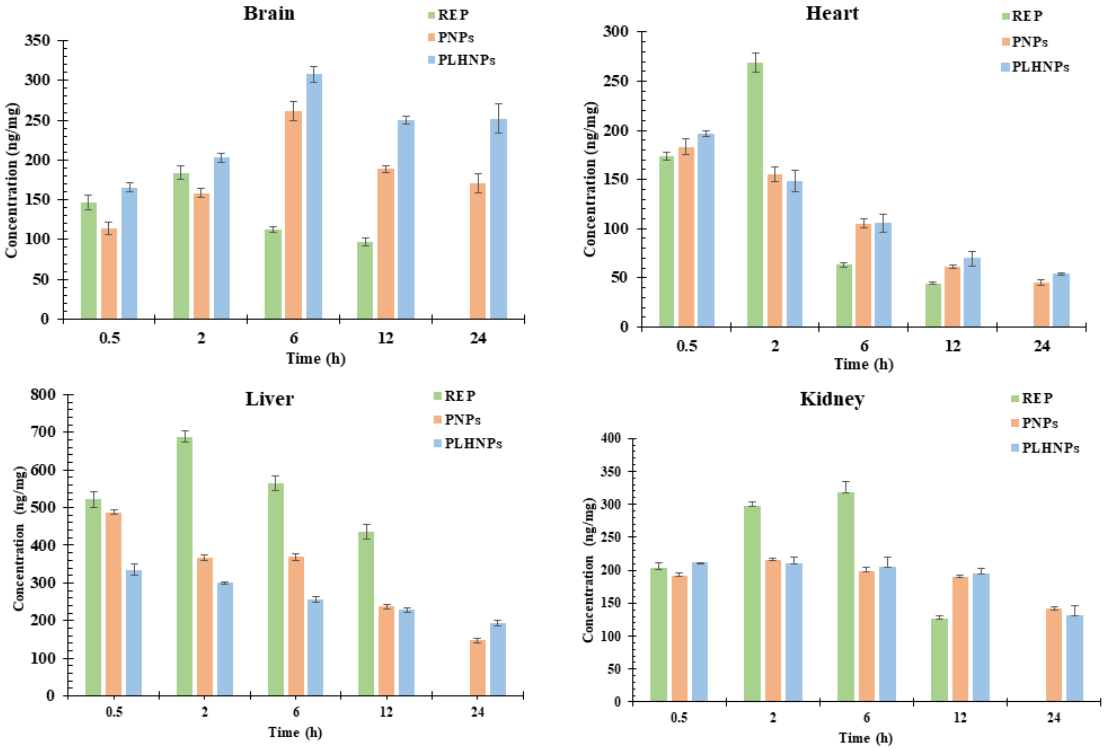

Fig.4.26: Biodistribution study of REP, PNPs, and PLHNPs on brain, heart, liver, and kidney.

4.4.9 Pharmacodynamic study

4.4.9.1 Estimation of neurochemical parameters

After the treatment period on HFD+STZ-induced wistar rats, the effect of REP, PNPs and PLHNPs were measured on neurochemical parameters such as BDNF, Aβ, and tau protein as shown in Fig.4.27 A-C. The BDNF level in the DC group was significantly ($p<0.001$) decreased than the NC group but after the treatment with REP, PNPs and PLHNPs a significant ($p<0.05$) amelioration was observed. The consistent amelioration of BDNF levels has resulted more in PLHNPs than REP.

Furthermore, Aβ deposition and hyperphosphorylation of tau proteins are the hallmarks of neurodegeneration and are crucial to the pathogenesis of AD. Thus, the potential effect of REP PNPs and PLHNPs were showed a significant ($p<0.001$) upregulation in the levels of Aβ and tau proteins in DC than the NC group. After treatment with REP, PNPs and PLHNPs, a significant attenuation was observed in comparison with the DC group.

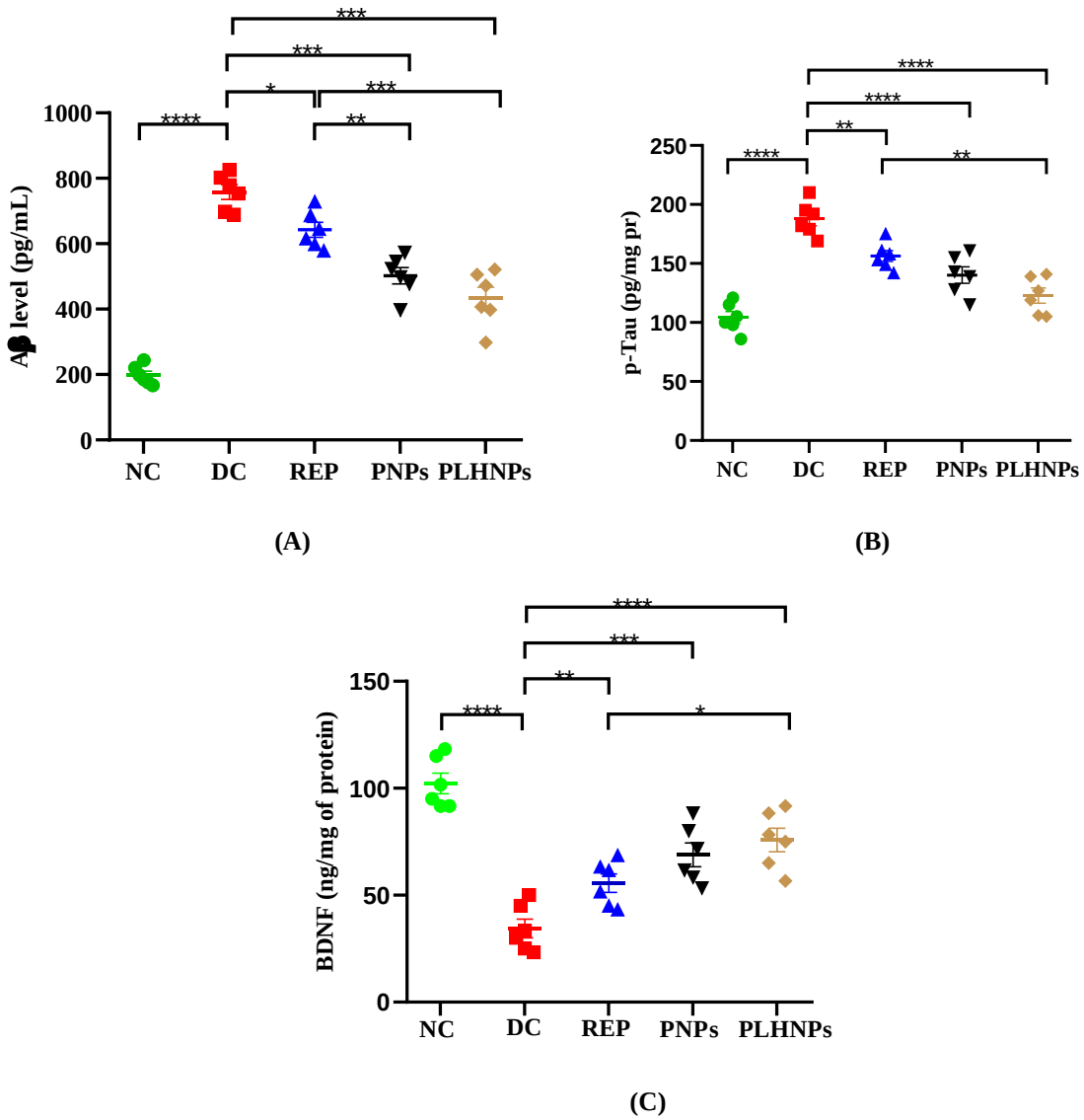

Fig.4.27: *In vivo* estimation of neurochemical parameters to understand the effect of REP,PNPs and PLHNPs after the treatment (A) Aβ level; (B) p-Tau; (C) BDNF level in brain homogenate of HFD+STZ induced wistar rats, data are represented in (mean ± SEM, n=6 rats per group). * Indicates *P< 0.05;* ** *P< 0.01,* *** *P< 0.001,* **** *P< 0.0001* by one-way ANOVA followed by Tukey's post hoc multiple comparison test

4.4.9.2 Estimation of inflammatory cytokines

The effect of REP, PNPs and PLHNPs on inflammatory cytokines (TNF-α and IL-6) was estimated in HFD+STZ-induced wistar rats (Fig.4.28 A&B). The significant (p< 0.0001) upregulation of levels was observed in DC compared to NC rats. Moreover, the REP, PNPs and PLHNPs administration for 4 weeks was reduces the levels than the DC group but PLHNPs showed a significant (p<0.001) suppression as compared to REP.

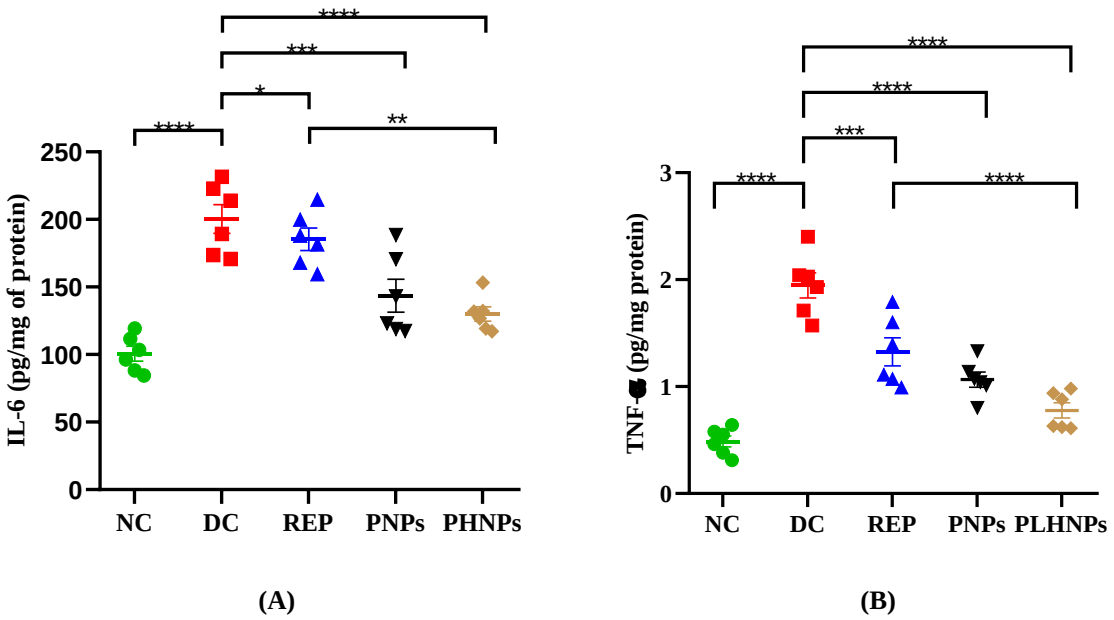

Fig.4.28: *In vivo* estimation of neurochemical parameters to understand the effect of REP, PNPs and PLHNPs after the treatment (A) IL-6; and (B) TNF-α level in brain homogenate of HFD+STZ induced wistar rats, data are represented in (mean ± SEM, n=6 rats per group). * Indicates *P< 0.05;* ** *P< 0.01*, *** *P< 0.001*, **** *P< 0.0001* by one-way ANOVA followed by Tukey's post hoc multiple comparison test

4.4.9.3 Morri's water maze (MWM)

The effect of REP, PNPs and PLHNPs were measured for the estimation of spatial memory. The mean escape latency in all groups was recorded after the 4 days of training and observed a gradual attenuation in MWM analysis. Though in the DC group, the mean escape latency was significantly ($p<0.001$) higher with the NC group and decrement was observed after treatment with REP and PLHNPs as shown in Fig.4.32. A. In the second part of the analysis, the hidden platform was removed to perform a probe trial test, where DC group rats were unable to identify the exact location of the platform and spent less time in that quadrant than the NC group rats. However, after the treatment with REP, PNPs and PLHNPs, rats were able to recall the exact position of the platform and spend more time in that quadrant which indicates memory improvement (Fig.4.32. B).

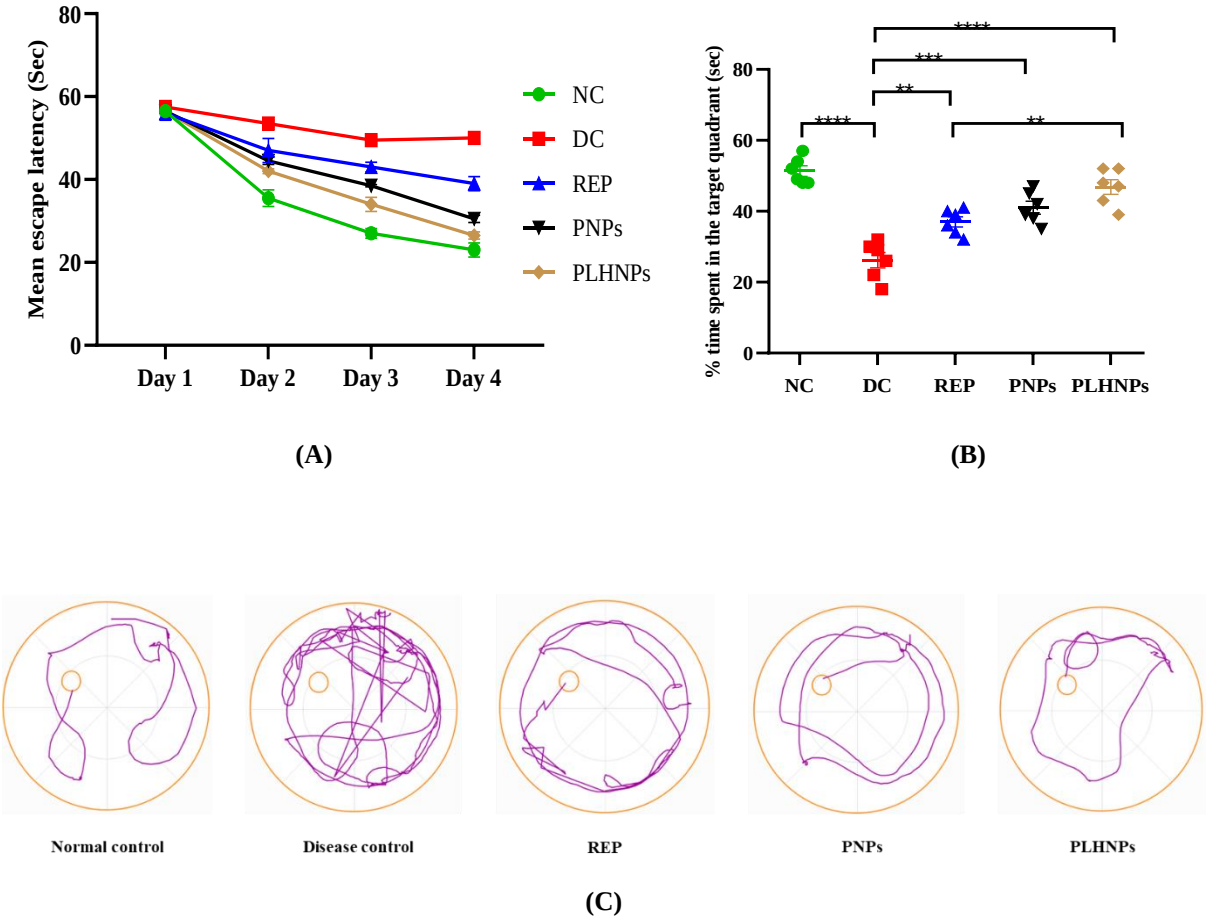

Fig.4.32: Estimation of (A) mean escape latency, (B) time spent in the same quadrant, and (C) representation of track plot for Morri's water maze task. Data are represented in (mean ± SEM, n=6 rats per group). data are represented in (mean ± SEM, n=6 rats per group). * Indicates *P< 0.05; ** P< 0.01, *** P< 0.001, **** P< 0.0001* by one-way ANOVA followed by Tukey's post hoc multiple comparison test

In summary, the conventional preparations suffer from certain limitations and do not provide sustained effects therefore novel carriers were developed which could meet requirements for drug delivery systems. A nanoparticulate drug delivery system has been proposed to improve the limitations of the conventional system. PNPs and PLHNPs were formulated and evaluated as effective nanocarrier systems for the brain delivery of REP via oral administration. The evaluation of both nanoparticles was done by performing various physicochemical, *in vitro,* and *in vivo* studies. Though from physicochemical studies no significant differences were observed as both have PS < 150nm, PDI< 0.3, and fulfill the morphological criteria of shape, and size. However, through the results, it was observed that PLHNPs released REP in a controlled manner, with high effective permeability in the intestine and brain. Moreover, in cellular studies, the PLHNPs were found to be more effective than PNPs and have a significant effect on pharmacokinetic parameters. In biodistribution and pharmacodynamic studies of PLHNPs, a significant effect on the neurochemicals, inflammatory biomarkers, and oxidative

parameters was observed as compared to PNPs. The core-shell structure of PLHNPs which efficiently loads the poorly water-soluble active ingredient and lipid monolayer reduces the outward diffusion of the drug and provides stability. Further, the outer layer of lipid PEG enhances systemic circulation and protects against immune recognition. Hence, it was revealed that PLHNPs were more efficient for the brain delivery of REP by oral administration than the PNPs.

5. Impact of Research:

The prevalence of AD and MetS on the rise, the research outcomes resonate as a significant breakthrough in the field. The confirmation of REP's neuroprotective attributes and its efficacy in addressing the tandem challenges of AD and MetS underscore its potential to revolutionize therapeutic strategies. This holds particular significance in an era where these conditions are becoming increasingly prevalent, thus elevating the need for innovative and effective interventions. Moreover, the study's insights shed light on new horizons for research and development. The efficacy of REP prompts a broader investigation into the therapeutic benefits of other anti-diabetic agents under similar conditions, thereby paving the way for an expanded arsenal of treatment options. Additionally, the research's implications extend to drug delivery strategies, formulation techniques, and manufacturing processes. By optimizing these aspects, the study sets the stage for enhancing treatment accessibility, cost-effectiveness, and patient adherence, all of which are pivotal in the context of increasing disease burden.

The research's multi-faceted approach also underscores the importance of patient-centered care. It advocates for dosage forms that enhance patient compliance, thereby improving treatment efficacy and overall health outcomes. The research is a clarion call for comprehensive, innovative, and patient-centric solutions in the face of the mounting challenges posed by AD and MetS. Its findings resonate as a beacon of hope, guiding the trajectory of medical research and practice in a direction that aligns with the pressing needs of our times.

6. Literature reference:

1. Lanktree MB, Hegele RA. Metabolic Syndrome. *Genomic Precis Med Cardiovasc Dis Third Ed*. Published online January 1, 2018:47-63. doi:10.1016/B978-0-12-801812-5.00015-9

2. Rochlani Y, Pothineni NV, Kovelamudi S, Mehta JL. Metabolic syndrome: pathophysiology, management, and modulation by natural compounds. *Ther Adv Cardiovasc Dis*. 2017;11(8):215. doi:10.1177/1753944717711379

3. Akhtar A, Sah SP. Insulin signaling pathway and related molecules: Role in neurodegeneration and Alzheimer's disease. *Neurochem Int*. 2020;135. doi:10.1016/j.neuint.2020.104707

4. Mittal K, Mani RJ, Katare DP. Type 3 Diabetes: Cross Talk between Differentially Regulated Proteins of Type 2 Diabetes Mellitus and Alzheimer's Disease. *Sci Reports 2016 61*. 2016;6(1):1-8. doi:10.1038/srep25589

5. Jeong S. Molecular and Cellular Basis of Neurodegeneration in Alzheimer's Disease. *Mol Cells*. 2017;40(9):613. doi:10.14348/MOLCELLS.2017.0096

6. Huang J, Huang N, Cui D, Shi J, Qiu Y. Clinical antidiabetic medication used in Alzheimer's disease: From basic discovery to therapeutics development. *Front Aging Neurosci*. 2023;15. doi:10.3389/FNAGI.2023.1122300

7. Scott LJ. Repaglinide. *Drugs 2012 722*. 2012;72(2):249-272. doi:10.2165/11207600-000000000-00000

8. Motawi TK, Al-Kady RH, Senousy MA, Abdelraouf SM. Repaglinide Elicits a Neuroprotective Effect in Rotenone-Induced Parkinson's Disease in Rats: Emphasis on Targeting the DREAM-ER Stress BiP/ATF6/CHOP Trajectory and Activation of Mitophagy. *ACS Chem Neurosci*. Published online 2022. doi:10.1021/ACSCHEMNEURO.2C00656/ASSET/IMAGES/MEDIUM/CN2C00656_0011.GIF

9. Naranjo JR, Zhang H, Villar D, et al. Activating transcription factor 6 derepression mediates neuroprotection in Huntington disease. *J Clin Invest*. 2016;126(2):627-638. doi:10.1172/JCI82670

10. Gorantla S, Wadhwa G, Jain S, et al. Recent advances in nanocarriers for nutrient delivery. *Drug Deliv Transl Res*. 2021;1:3. doi:10.1007/s13346-021-01097-z

11. Alexander A, Agrawal M, Uddin A, et al. Recent expansions of novel strategies towards the drug targeting into the brain. *Int J Nanomedicine*. 2019;14:5895. doi:10.2147/IJN.S210876

12. Wadhwa G, Krishna KV, Dubey SK, Taliyan R. PEGylated Polymer–Lipid Hybrid Nanoparticles to Enhance *In Vivo* Exposure and Uptake of Repaglinide in Brain Cells to Treat Diabetes-Linked Neurodegenerative Disorders. *ACS Appl Nano Mater*. Published online February 8, 2023. doi:10.1021/ACSANM.2C05272

13. Zhang J, Wang D, Wu Y, et al. Lipid−Polymer Hybrid Nanoparticles for Oral Delivery of Tartary Buckwheat Flavonoids. Published online 2018. doi:10.1021/acs.jafc.8b00714

14. Gajbhiye KR, Pawar A, Mahadik KR, Gajbhiye V. PEGylated nanocarriers: A promising tool for targeted delivery to the brain. *Colloids Surfaces B Biointerfaces*. 2020;187:110770. doi:10.1016/J.COLSURFB.2019.110770

15. Bagaméry F, Varga K, Kecsmár K, Vincze I, Szökő É, Tábi T. Lack of insulin resistance in response to streptozotocin treatment in neuronal SH-SY5Y cell line. *J Neural Transm*. 2020;127(1):71-80. doi:10.1007/S00702-019-02118-5

16. Zamani M, Sadeghizadeh M, Behmanesh M, Najafi F. Dendrosomal curcumin increases expression of the long non-coding RNA gene MEG3 via up-regulation of epi-miRs in hepatocellular cancer. *Phytomedicine*. 2015;22(10):961-967. doi:10.1016/j.phymed.2015.05.071

17. Wang J, Yin J, Song Y, Zhang L, … YR-J of D, 2014 undefined. Brain aging and AD-like pathology in streptozotocin-induced diabetic rats. *hindawi.com*. Accessed December 26, 2022. https://www.hindawi.com/journals/jdr/2014/796840/

18. Sun P, Ortega G, Tan Y, et al. Streptozotocin impairs proliferation and differentiation of adult hippocampal neural stem cells in vitro-correlation with alterations in the expression of proteins associated with the insulin system. *Front Aging Neurosci*. 2018;10(MAY). doi:10.3389/FNAGI.2018.00145/FULL

19. Hattangady NG, Rajadhyaksha MS. A brief review of in vitro models of diabetic neuropathy. *Int J Diabetes Dev Ctries*. 2009;29(4):143-149. doi:10.4103/0973-3930.57344

20. Karavelioglu Z, Cakir-koc R. International Journal of Biological Macromolecules Preparation of chitosan nanoparticles as Ginkgo Biloba extract carrier : In vitro neuroprotective effect on oxidative stress-induced human. *Int J Biol Macromol*. 2021;192(October):675-683. doi:10.1016/j.ijbiomac.2021.10.023

21. Wesén E, Jeffries GDM, Dzebo MM, Esbjörner EK. Endocytic uptake of monomeric amyloid-β peptides is clathrin- and dynamin-independent and results in selective accumulation of Aβ(1-42) compared to Aβ(1-40). *Sci Rep*. 2017;7(1). doi:10.1038/S41598-017-02227-9

22. Kang S, Kim CH, Jung H, Kim E, Song HT, Lee JE. Agmatine ameliorates type 2 diabetes induced-Alzheimer's disease-like alterations in high-fat diet-fed mice via reactivation of blunted insulin signalling. *Neuropharmacology*. 2017;113:467-479. doi:10.1016/j.neuropharm.2016.10.029

23. Park KA, Jin Z, Lee JY, et al. Long-lasting exendin-4 fusion protein improves memory deficits in high-fat diet/streptozotocin-induced diabetic mice. *Pharmaceutics*. 2020;12(2):1-18. doi:10.3390/pharmaceutics12020159

24. Wadhwa G, Krishna KV, Taliyan R, et al. Pre-clinical pharmacokinetic and pharmacodynamic modelling study of 4-hydroxyisoleucine using validated ultra-performance liquid chromatography-tandem mass spectrometry. *RSC Adv*. 2020;10(10):5525-5532. doi:https://doi.org/10.1039/c9ra08121f

25. Narender T, Puri A, Shweta, et al. 4-Hydroxyisoleucine an unusual amino acid as antidyslipidemic and antihyperglycemic agent. *Bioorg Med Chem Lett*. 2006;16(2):293-296. doi:10.1016/J.BMCL.2005.10.003

26. Krishna KV, Saha RN, Dubey SK. Biophysical, Biochemical, and Behavioral Implications of ApoE3 Conjugated Donepezil Nanomedicine in a Aβ1-42Induced Alzheimer's Disease Rat Model. *ACS Chem Neurosci*. 2020;11(24):4139-4151. doi:10.1021/acschemneuro.0c00430

27. Sarathlal KCS, Kakoty V, Krishna KV, Dubey SK, Chitkara D, Taliyan R.

Neuroprotective Efficacy of Co-Encapsulated Rosiglitazone and Vorinostat Nanoparticle on Streptozotocin Induced Mice Model of Alzheimer Disease. *ACS Chem Neurosci*. 2021;12(9):1528-1541. doi:10.1021/ACSCHEMNEURO.1C00022/ASSET/IMAGES/MEDIUM/CN1C00022_M001.GIF

28. Sharma S, Taliyan R. Epigenetic modifications by inhibiting histone deacetylases reverse memory impairment in insulin resistance induced cognitive deficit in mice. *Neuropharmacology*. 2016;105:285-297. doi:10.1016/J.NEUROPHARM.2016.01.025

29. Kakoty V, K C S, Dubey SK, Yang CH, Taliyan R. Neuroprotective Effects of Trehalose and Sodium Butyrate on Preformed Fibrillar Form of α-Synuclein-Induced Rat Model of Parkinson's Disease. *ACS Chem Neurosci*. 2021;12(14):2643-2660. doi:10.1021/ACSCHEMNEURO.1C00144

30. Kakoty V, Sarathlal KC, Yang CH, Kumari S, Dubey SK, Taliyan R. Neuroprotective Effect of Lentivirus-Mediated FGF21 Gene Delivery in Experimental Alzheimer's Disease is Augmented when Concerted with Rapamycin. *Mol Neurobiol*. 2022;59(5):2659-2677. doi:10.1007/S12035-022-02741-6

31. Aslani MR, Ghobadi H, Panahpour H, Ahmadi M, Khaksar M, Heidarzadeh M. Modification of lung endoplasmic reticulum genes expression and NF-kB protein levels in obese ovalbumin-sensitized male and female rats. *Life Sci*. 2020;247. doi:10.1016/J.LFS.2020.117446

32. Pillai-Kastoori L, Schutz-Geschwender AR, Harford JA. A systematic approach to quantitative Western blot analysis. *Anal Biochem*. 2020;593:113608. doi:10.1016/J.AB.2020.113608

33. Lee K, Lee J, Park J, … TH-E& molecular, 2008 undefined. Low energy proton beam induces tumor cell apoptosis through reactive oxygen species and activation of caspases. *nature.com*. Accessed January 3, 2023. https://www.nature.com/articles/emm200814

34. Krishna KV, Saha RN, Puri A, Viard M, Shapiro BA, Dubey SK. Pre-clinical compartmental pharmacokinetic modeling of 2-[1-hexyloxyethyl]-2-devinyl pyropheophorbide-a (HPPH) as a photosensitizer in rat plasma by validated HPLC method. *Photochem Photobiol Sci*. Published online 2019. doi:10.1039/C8PP00339D

35. Wadhwa G, Krishna KV, Dubey SK, Taliyan R. Development and validation of RP-HPLC method for quantification of repaglinide in mPEG-PCL polymeric nanoparticles: QbD-driven optimization, force degradation study, and assessment of in vitro release mathematic modeling. *Microchem J*. 2021;168:106491. doi:10.1016/J.MICROC.2021.106491

36. Jiang L, Wee Lee H, Chye Joachim Loo S. Therapeutic lipid-coated hybrid nanoparticles against bacterial infections. Published online 2020. doi:10.1039/c9ra10921h

37. Yalcin TE, Ilbasmis-Tamer S, Takka S. Development and characterization of gemcitabine hydrochloride loaded lipid polymer hybrid nanoparticles (LPHNs) using central composite design. *Int J Pharm*. 2018;548(1):255-262. doi:10.1016/j.ijpharm.2018.06.063

38. Pallagi E, Ismail R, Paál TL, Csóka I. Initial Risk Assessment as part of the Quality by Design in peptide drug containing formulation development. *Eur J Pharm Sci*. 2018;122:160-169. doi:10.1016/J.EJPS.2018.07.003

39. Wu L, Zhao L, Su X, Zhang P, Ling G. Repaglinide-loaded nanostructured lipid carriers with different particle sizes for improving oral absorption: preparation, characterization, pharmacokinetics, and in situ intestinal perfusion. *https://doi.org/101080/1071754420191689313*. 2019;27(1):400-409. doi:10.1080/10717544.2019.1689313

40. Eriksen JN, Luu AY, Dragsted LO, Arrigoni E. Adaption of an in vitro digestion method to screen carotenoid liberation and in vitro accessibility from differently processed spinach preparations Adaption of an in vitro digestion method to screen carotenoid liberation and in vitro accessibility from di. *Food Chem*. 2016;(November). doi:10.1016/j.foodchem.2016.11.146

41. Li Z, Peng S, Chen X, Zhu Y, Zou L, Liu W. Pluronics modi fi ed liposomes for curcumin encapsulation : Sustained release , stability and bioaccessibility. 2018;108(December 2017):246-253. doi:10.1016/j.foodres.2018.03.048

42. Strindberg S, Plum J, Stie MB, et al. Effect of supersaturation on absorption of indomethacin and tadalafil in a single pass intestinal perfusion rat model, in the absence and presence of a precipitation inhibitor. *Eur J Pharm Biopharm*. 2020;151:108-115. doi:10.1016/J.EJPB.2020.03.019

43. Dezani TM, Dezani AB, Junior JBDS, Serra CHDR. Single-Pass Intestinal Perfusion (SPIP) and prediction of fraction absorbed and permeability in humans: A study with antiretroviral drugs. *Eur J Pharm Biopharm*. 2016;104:131-139. doi:10.1016/J.EJPB.2016.04.020

44. Dezani TM, Dezani AB, Junior JBDS, Serra CHDR. Single-Pass Intestinal Perfusion (SPIP) and prediction of fraction absorbed and permeability in humans: A study with antiretroviral drugs. *Eur J Pharm Biopharm*. 2016;104:131-139. doi:10.1016/J.EJPB.2016.04.020

45. Konsoula R, Jung M. In Vitro Plasma Stability, Permeability and Solubility of Mercaptoacetamide Histone Deacetylase Inhibitors. doi:10.1016/j.ijpharm.2008.05.001

46. Strindberg S, Plum J, Stie MB, et al. Effect of supersaturation on absorption of indomethacin and tadalafil in a single pass intestinal perfusion rat model, in the absence and presence of a precipitation inhibitor. *Eur J Pharm Biopharm*. 2020;151:108-115. doi:10.1016/J.EJPB.2020.03.019

47. Wu L, Zhao L, Su X, Zhang P, Ling G. Repaglinide-loaded nanostructured lipid carriers with different particle sizes for improving oral absorption: preparation, characterization, pharmacokinetics, and *in situ* intestinal perfusion. *Drug Deliv*. Published online November 15, 2019:1-10. doi:10.1080/10717544.2019.1689313

48. Graverini G, Piazzini V, Landucci E, et al. Solid lipid nanoparticles for delivery of andrographolide across the blood-brain barrier: in vitro and in vivo evaluation. *Colloids Surfaces B Biointerfaces*. 2018;161:302-313. doi:10.1016/j.colsurfb.2017.10.062

49. Radan M, Djikic T, Obradovic D, Nikolic K. Application of in vitro PAMPA technique and in silico computational methods for blood-brain barrier permeability prediction of novel CNS drug candidates. *Eur J Pharm Sci*. 2022;168:106056. doi:10.1016/J.EJPS.2021.106056

50. Wadhwa G, Venkata Krishna K, Kumar Dubey S, Taliyan R. Design and biological evaluation of Repaglinide loaded polymeric nanocarriers for diabetes linked neurodegenerative disorder: QbD-driven optimization, in situ, in vitro and in vivo investigation. *Int J Pharm*. 2023;636:122824. doi:10.1016/J.IJPHARM.2023.122824

51. Park J, Won J, Seo J, et al. Streptozotocin Induces Alzheimer's Disease-Like Pathology in Hippocampal Neuronal Cells via CDK5/Drp1-Mediated Mitochondrial Fragmentation. *Front Cell Neurosci*. 2020;14. doi:10.3389/FNCEL.2020.00235/FULL

52. Krishna KV, Wadhwa G, Alexander A, et al. Design and Biological Evaluation of Lipoprotein-Based Donepezil Nanocarrier for Enhanced Brain Uptake through Oral Delivery. *ACS Chem Neurosci*. 2019;10(9):4124-4135. doi:10.1021/acschemneuro.9b00343

53. Garg NK, Tyagi RK, Sharma G, et al. Functionalized Lipid−Polymer Hybrid Nanoparticles Mediated Codelivery of Methotrexate and Aceclofenac: A Synergistic Effect in Breast Cancer with Improved Pharmacokinetics Attributes. Published online 2017. doi:10.1021/acs.molpharmaceut.6b01148

54. Adamo G, Campora S, Ghersi G. Functionalization of nanoparticles in specific targeting and mechanism release. *Nanostructures Nov Ther Synth Charact Appl*. Published online January 1, 2017:57-80. doi:10.1016/B978-0-323-46142-9.00003-7

55. Yang H, Zhai B, Fan Y, et al. Intestinal absorption mechanisms of araloside A in situ single-pass intestinal perfusion and in vitro Caco-2 cell model. *Biomed Pharmacother*. 2018;106:1563-1569. doi:10.1016/J.BIOPHA.2018.07.117

56. Garg NK, Singh B, Sharma G, et al. Development and characterization of single step self-assembled lipid polymer hybrid nanoparticles for effective delivery of methotrexate. *RSC Adv*. 2015;5(77):62989-62999. doi:10.1039/c5ra12459j

57. Simon A, Darcsi A, Kéry Á, Riethmüller E. Blood-brain barrier permeability study of ginger constituents. *J Pharm Biomed Anal*. 2020;177:112820. doi:10.1016/J.JPBA.2019.112820

58. Mandal B, Mittal NK, Balabathula P, Thoma LA, Wood GC. *Development and in Vitro Evaluation of Core-Shell Type Lipid-Polymer Hybrid Nanoparticles for the Delivery of Erlotinib in Non-Small Cell Lung Cancer*. Vol 81. Elsevier B.V.; 2016. doi:10.1016/j.ejps.2015.10.021